Geochemistry Geophysics Geosystems G3

Article
Volume 12, Number 4
13 April 2011
Q04S30, doi:10.1029/2010GC003477
ISSN: 1525-2027

Published by AGU and the Geochemical Society

The steeply subducting edge of the Cocos Ridge: Evidence from receiver functions beneath the northern Talamanca Range, south-central Costa Rica

Y. Dzierma, W. Rabbel, and M. M. Thorwart
Abteilung Geophysik, Institut für Geowissenschaften, Christian-Albrechts-Universität zu Kiel, Otto-Hahn-Platz 1, D-24118 Kiel, Germany (ydzierma@geophysik.uni-kiel.de)

SFB 574, Christian-Albrechts-Universität zu Kiel, Otto-Hahn-Platz 1, D-24118 Kiel, Germany

E. R. Flueh
Leibniz-Institut für Meereswissenschaften an der Universität Kiel (IFM-GEOMAR), Wischhofstrasse 1-3, D-24148 Kiel, Germany

SFB 574, Christian-Albrechts-Universität zu Kiel, D-24148 Kiel, Germany

M. M. Mora
Escuela Centroamericana de Geología, Universidad de Costa Rica, Apartado Postal 214-2060, Ciudad Universitaria Rodrigo Facio, San Pedro de Montes de Oca, San José, Costa Rica

G. E. Alvarado
Área de Amenazas y Auscultación Sísmica y Volcánica, Instituto Costarricense de Electricidad, Apdo. 10032-1000, San José, Costa Rica

[1] The deep structure of the south-central Costa Rican subduction zone has not been studied in great detail so far because large parts of the area are virtually inaccessible. We present a receiver function study along a transect of broadband seismometers through the northern flank of the Cordillera de Talamanca (south Costa Rica). Below Moho depths, the receiver functions image a dipping positive conversion signal. This is interpreted as the subducting Cocos Plate slab, compatible with the conversions in the individual receiver functions. In finite difference modeling, a dipping signal such as the one imaged can only be reproduced by a steeply (80°) dipping structure present at least until a depth of about 70–100 km; below this depth, the length of the slab cannot be determined because of possible scattering effects. The proposed position of the slab agrees with previous results from local seismicity, local earthquake tomography, and active seismic studies, while extending the slab location to greater depths and steeper dip angle. Along the trench, no marked change is observed in the receiver functions, suggesting that the steeply dipping slab continues until the northern flank of the Cordillera de Talamanca, in the transition region between the incoming seamount segment and Cocos Ridge. Considering the time predicted for the establishment of shallow angle underthrusting after the onset of ridge collision, the southern Costa Rican subduction zone may at present be undergoing a reconfiguration of subduction style, where the transition to shallow underthrusting may be underway but still incomplete.

Components: 7800 words, 18 figures, 1 table.

Keywords: south-central Costa Rican subduction zone; seismometer transect through northern Cordillera de Talamanca; receiver functions; subduction of the Cocos Ridge edge.

Index Terms: 7240 Seismology: Subduction zones (1207, 1219, 1240); 8170 Tectonophysics: Subduction zone processes (1031, 3060, 3613, 8413); 7299 Seismology: General or miscellaneous.

Received 21 December 2010; **Revised** 15 February 2011; **Accepted** 21 February 2011; **Published** 13 April 2011.

Dzierma, Y., W. Rabbel, M. M. Thorwart, E. R. Flueh, M. M. Mora, and G. E. Alvarado (2011), The steeply subducting edge of the Cocos Ridge: Evidence from receiver functions beneath the northern Talamanca Range, south-central Costa Rica, *Geochem. Geophys. Geosyst.*, *12*, Q04S30, doi:10.1029/2010GC003477.

Theme: Central American Subduction System
Guest Editors: G. Alvarado, K. Hoernle, and E. Silver

1. Introduction

[2] While the Central American subduction zone (Figure 1) has been studied in great detail in recent years, its onshore terminus in south Costa Rica and Panama has received relatively little attention due to the fact that large parts of this region are covered in a dense jungle and are hence hardly accessible. Together with the scarcity of available data, the complex tectonic setting of this area complicates interpretation even further. The eastern end of the Cocos Plate, bordering the Nazca Plate along the Panama Fracture Zone (PFZ), is overlain by the aseismic Cocos Ridge, a buoyant ridge of up to 20 km crustal thickness formed as the trace of the Galápagos hot spot [*Sallarès et al.*, 2003]. The collision of the Cocos Ridge with the Middle American Trench (MAT) has been argued to have choked subduction, causing recent uplift of the Cordillera de Talamanca and a pronounced lack of volcanic activity and deep seismicity in this region [*Collins et al.*, 1995; *de Boer et al.*, 1995; *Kolarsky et al.*, 1995; *Protti et al.*, 1995]. Whether or not this southern segment of the Cocos Plate underplates or subducts, and if so, at which angle, is still unknown (compare Figure 2). Equally debated is the proposed presence of a slab window beneath the Cordillera de Talamanca [*Johnston and Thorkelson*, 1997; *Abratis and Wörner*, 2001]. Furthermore, the Caribbean Plate has been shown to underthrust beneath the northern boundary of the Panama Microplate [*Camacho et al.*, 2010] and may form a backstop against which the Cocos Ridge segment of the Cocos Plate may collide during subduction/underplating.

[3] The aim of this work is to shed some light on the deeper structure in south-central Costa Rica, based on a broadband transect through the region where the continuation of the slab is still unknown (Figure 2). While more measurements are desirable, this study presents one of the first approaches to image the deep structure under the northern edge of the Talamanca Range, where coverage of previous seismicity and tomography studies has been limited.

[4] We start with an overview of the regional tectonic setting, which will provide the necessary background for the observations and interpretation. The main results of this study are based on a receiver function analysis. They show the existence of dipping structure below the continental Moho, which is interpreted as the steeply subducting Cocos Plate slab. This result is confirmed by forward modeling. We compare our results with previously known structural characteristics and discuss the implications for Cocos Ridge subduction.

2. Tectonic Framework

2.1. Panama Microplate and Subducting Cocos Plate

[5] The collision of the Middle American land bridge with south America about 7 Ma ago resulted in the formation of the Panama Microplate, comprising south Costa Rica and Panama [*Kellogg and Vega*, 1995]. The tectonic escape created the characteristic shape of the Panama isthmus and has been held responsible by some authors for the uplift and closure of the Central American land bridge [e.g., *Burke*, 1988], which others have attributed to shallow angle underthrusting of the Cocos Ridge (this mainly depends on when Cocos Ridge collision is believed to have started).

[6] In addition to the near-normal subduction of the Cocos Plate beneath the southern edge of the Panama Microplate along the Middle America Trench (MAT) (Figure 1) [*Barckhausen et al.*, 2001; *deMets et al.*, 1990, 1994], the northern limit of the Panama Microplate is underthrust by the Caribbean Plate in the so-called north Panama

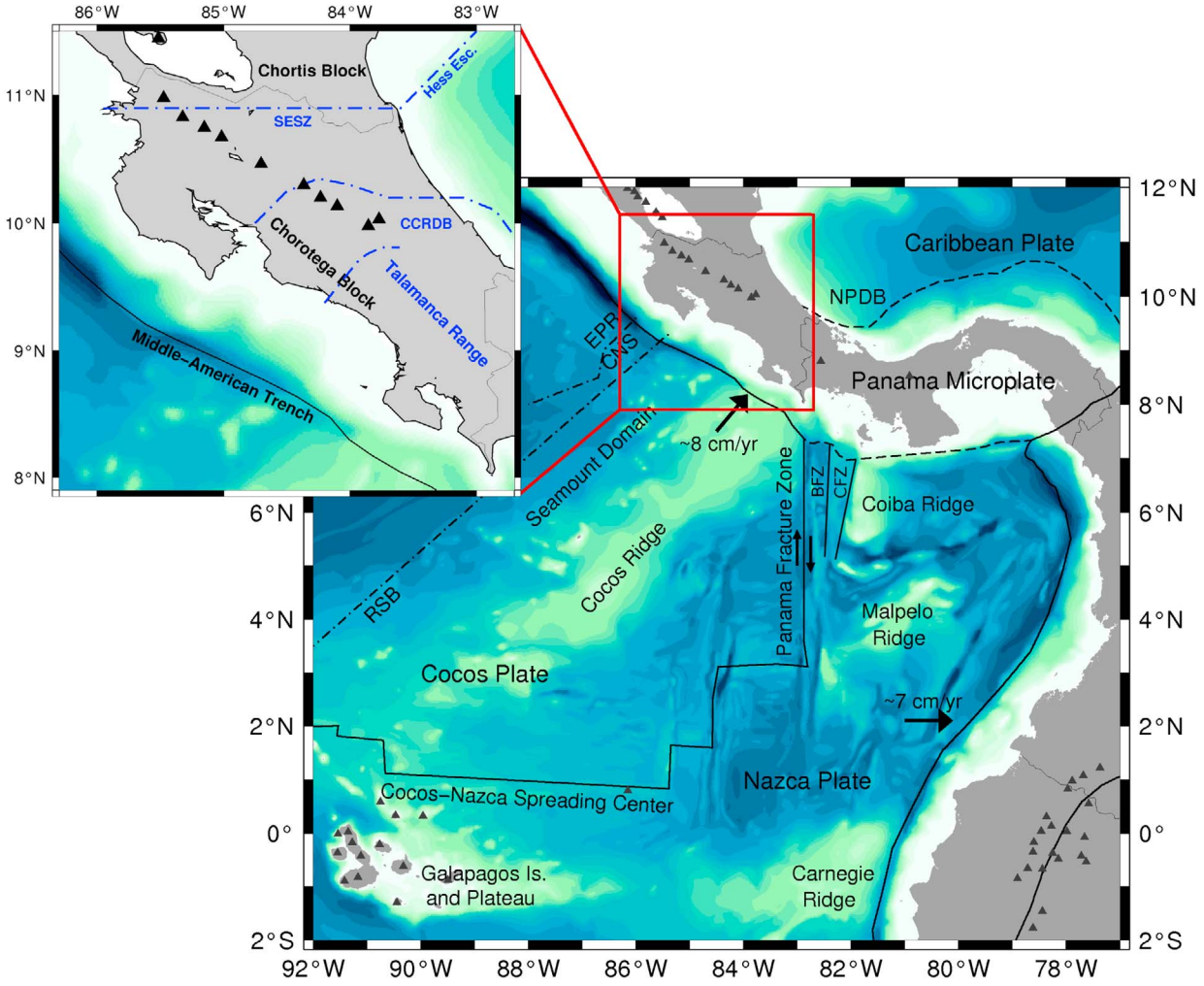

Figure 1. Tectonic overview of southern Central America and the eastern Panama Basin. Volcanoes are indicated by dark triangles. The boundary between crust produced at the east Pacific Rise (EPR) and at the Cocos-Nazca Spreading Center (CNS) is shown schematically. Below is the rough-smooth boundary (RSB), south of which commences the seamount segment. The Cocos Ridge is bordered by the Panama Fracture Zone and the adjacent Balboa Fracture Zone (BFZ) and Coiba Fracture Zone (CFZ). Plate boundaries are based on *Bird* [2003]. The enlarged box shows Costa Rica, with the main fault zones (schematic): the central Costa Rica Deformed Belt (CCRDB) [*Lewis et al.*, 2008] as a continuation of the north Panama Deformed Belt (NPDB) and the Santa Elena Suture Zone (SESZ) in prolongation of the Hess Escarpment (Hess Esc.) [*Dengo*, 1985; *Barckhausen et al.*, 2001].

Deformed Belt (NPDB [*Adamek et al.*, 1988; *Camacho et al.*, 2010]). The northwest boundary of the Panama Block is unclear and has been speculated to run along a fault system in central Costa Rica (the central Costa Rica Deformed Belt (CCRDB) [*Mann et al.*, 2007; *Marshall et al.*, 2000; *Montero*, 2001]) or else to occur as far north as the Santa Elena Suture Zone (SESZ) [*Dengo*, 1985; *Escalante*, 1990].

[7] The crust of the Cocos Plate is formed partly at the east Pacific Rise (EPR) and partly at the Cocos-Nazca spreading center (CNS). The boundary between the crust formed at the EPR and that formed at the CNS is termed the rough-smooth boundary (RSB) and impinges on the MAT off Nicoya Peninsula in north Costa Rica [*Hey*, 1977]. As a result of overprinting by the Galápagos hot spot trace and tectonic segmentation by the changing configuration of the CNS [*Barckhausen et al.*, 2001, 2008; *Hey*, 1977; *Meschede et al.*, 1998; *Meschede and Barckhausen*, 2000]), the Cocos Plate subducting off Costa Rica can been divided into three morphologically distinct regions [*von Huene et al.*, 1995, 2000]: (1) a smooth segment of igneous oceanic crust (20–25 Ma),

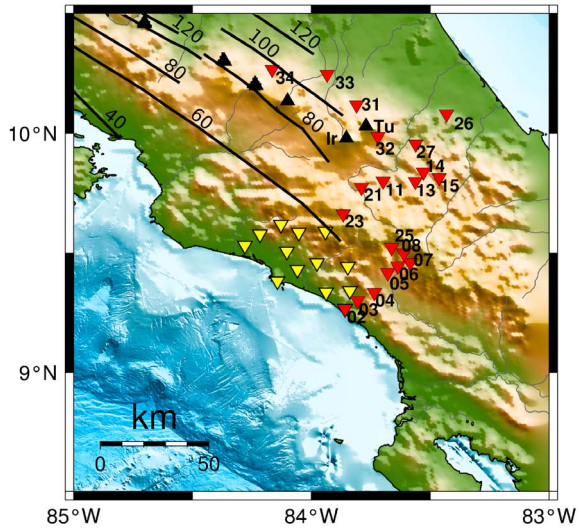

Figure 2. Talamanca Transect stations (red) used for the receiver function analysis and Quepos network (yellow, used by *Dinc et al.* [2010] to obtain local seismicity). Black triangles denote the principal volcanoes. Irazu (Ir) and Turrialba (Tu) mark the southern end of the volcanic chain in Costa Rica. Slab contours from *DeShon et al.* [2003] and *Protti et al.* [1995].

covered by sediments; (2) the seamount domain of 15–20 Ma oceanic crust covered 40% by seamounts; and (3) the Cocos Ridge (<15 Ma) overlying young oceanic crust. Both the seamount domain and Cocos Ridge were created by the Galápagos hot spot, and both are geochemically related [*Werner et al.*, 1999; *Hoernle et al.*, 2008; *Kokfelt et al.*, 2005]. The Cocos ridge trends N45°E, colliding with the trench offshore the Cordillera de Talamanca in southern Costa Rica. At its southern end the Cocos Ridge is cut by the PFZ, south of which lie two old transform faults, the Balboa Fracture Zone (BFZ) and the Coiba Fracture Zone (CFZ) bordering the Coiba Ridge.

2.2. The Central American Volcanic Arc

[8] The Central American Quaternary volcanic front extends for 1500 km from Guatemala to Panama, with a pronounced gap of 200 km length between Irazú-Turrialba in Costa Rica and Barú in Panama [*Carr*, 1984; *Carr and Stoiber*, 1990; *Feigenson and Carr*, 1993; *Leeman et al.*, 1994; *Carr et al.*, 2007] (also compare *Phipps Morgan et al.* [2008] for a recent review).

[9] In the volcanic gap of the Cordillera de Talamanca, Plio-Pleistocene and recent age volcanoes are absent, but adakites were emplaced between 3.6 and 1.9 Ma [*de Boer et al.*, 1995]. The gap in active volcanism has mainly been attributed to shallow underthrusting of the buoyant Cocos Ridge. In this case, no mantle wedge would be present where melt could be generated, explaining both the gap in active volcanism and the shortening and uplift of the Talamanca region [*Collins et al.*, 1995; *Corrigan et al.*, 1990; *Gardner et al.*, 1992; *Gräfe et al.*, 2002; *LaFemina et al.*, 2009; *McGeary et al.*, 1985; *Sitchler et al.*, 2007]. Even if melts are formed, *de Boer et al.* [1995] propose that the magmas might not be buoyant enough to rise through the thick and uplifted crust, being emplaced as plutons rather than erupted at the stratovolcanoes.

[10] While some authors have proposed partial melting of the warm (young) slab as a source for the adakites [*de Boer et al.*, 1995], particularly in the case of shallow angle underthrusting, this has been debated on the grounds of geothermal and isotopic data [*Johnston and Thorkelson*, 1997; *Abratis and Wörner*, 2001]. An alternative hypothesis would be heating of the slab edge as a consequence of Pacific mantle upwelling through a slab window, which may have been formed by the subduction of a spreading ridge or by slab breakoff [*Abratis*, 1998]. The absence of a subducting slab as a fluid reservoir would also explain the absence of active subduction zone volcanism. Recently, *Goss and Kay* [2006] have presented an alternative mixing model to create the observed adakite chemical characteristics, in which the Cocos Ridge would act to enhance subduction erosion of the Osa ophiolite and mélange and carry its geochemical signature into the subduction zone.

[11] Most of the aforementioned studies have relied on the presumed causal relationship of Cocos Ridge collision with uplift (also the closure of the land bridge), the shutdown of volcanism, adakite emplacement, etc. (for a compilation, see, e.g., *Kolarsky et al.* [1995]). This interpretation depends on the timing of Cocos Ridge collision with the trench, which is still debated. Estimates range from 0.5 to 8 Ma [*Collins et al.*, 1995; *Gardner et al.*, 1992; *Gräfe et al.*, 2002; *Lonsdale and Klitgord*, 1978; *Meschede et al.*, 1998; *Sallarès et al.*, 2003; *Silver et al.*, 1990]. *MacMillan et al.* [2004] use plate reconstructions to argue that the Cocos Ridge collision postdates many of the observed geological changes and cannot therefore be responsible. They contend that the spatial and temporal distribution of adakites, changes in sedimentation rates and basin depth, cessation of volcanism and geologic unconformities do not correlate with Cocos Ridge

subduction, but may be linked with Coiba Ridge subduction and the migration of the triple junction. The posterior entry of the Cocos Ridge into the MAT would then have exacerbated these effects.

2.3. Previous Seismic Experiments

[12] The shallow structure of the south Costa Rican margin was investigated by an onshore-offshore active seismic experiment along a transect passing through Dominical to Limón [*Stavenhagen*, 1998; *Stavenhagen et al.*, 1998]. In the upper plate, high crustal velocities in excess of 6.0 m/s were observed beneath the sedimentary cover, and the Moho was tentatively placed at 35 km depth. A receiver function study of the south-central Costa Rican land bridge [*Dzierma et al.*, 2010] could confirm the depth of the crustal interface and of the Moho observed by *Stavenhagen* [1998] close to the Caribbean coast, but showed considerable Moho topography under the Cordillera de Talamanca, in agreement with a thickened crustal root needed to isostatically compensate the high mountain range.

[13] The Cocos Plate observed in active seismic data [*Stavenhagen*, 1998; *Stavenhagen et al.*, 1998] was found to dip at an angle of 18° at a depth of 15–35 km. The subducting plate has a thick crust with pronounced magmatic layering in the upper crust. Above the slab, a thick (>5 km) low-velocity zone was observed, probably containing eroded margin wedge material. The slab dip in the upper 30–40 km depth was confirmed by *DeShon et al.* [2003] based on an interplate aftershock sequence in the Osa Peninsula region.

[14] In contrast to the relatively well-known crustal and shallow slab structure, the deeper structure of the subduction zone in this region has not yet been imaged with sufficient clarity. A study of the seismically defined Wadati-Benioff Zone (WBZ) in Costa Rica by *Protti et al.* [1994, 1995] showed that the maximum earthquake depth decreases from 220 km under Nicaragua to 50 km southeast of Punta Uvita (under Osa Peninsula). The shallowing of the observed seismicity was interpreted by *Protti et al.* [1994, 1995] as an indication for shallow angle underthrusting of the Cocos Ridge, consistent with results by *Burbach et al.* [1984] and *Guendel* [1986]. The decrease in maximum depth of seismicity observed by *Protti et al.* [1994, 1995] was explained by the younger and warmer incoming Cocos Plate (since slip may be aseismic [e.g., *de Boer et al.*, 1988; *Kirby et al.*, 1996]). The abrupt termination of the WBZ south of Punta Uvita may indicate the absence of a slab in this region, which is along the landward projection of the PFZ. On the basis of the study by *Protti et al.* [1994, 1995], the most widely accepted hypothesis presumed by most authors has been shallow angle underthrusting or underplating of the Cocos Ridge [e.g., *Abratis and Wörner*, 2001; *Fisher et al.*, 2004; *Kolarsky et al.*, 1995; *Peacock et al.*, 2004; *Rüpke et al.*, 2002].

[15] Observations of seismicity by *Husen et al.* [2003] confirm the subduction geometry of *Protti et al.* [1994, 1995], with a decrease in the maximum depth of seismicity toward south Costa Rica. A local earthquake tomography study based on this data could image the subducting Cocos Plate as a high-velocity anomaly in central Costa Rica down to 70 km depth, but failed to image the slab below 30 km depth in south Costa Rica. Here, the subducting plate appears as a low-velocity feature which seems to be colliding with a high-velocity backstop, possibly the Caribbean Plate underthrusting from the north.

[16] Underneath the northern edge of the Cordillera de Talamanca, sufficiently far from the slab edge, *Quintero and Kissling* [2001] record local seismicity dipping down to almost 120 km depth. Their localization has strong scatter, thereby making it hard to estimate the subduction angle, which ranges between 30° and 45° at depths greater than 30 km. This is in agreement with the profiles found by *Protti et al.* [1994, 1995] in the same region. Further south, *Arroyo* [2001] observed local seismicity below the Osa Peninsula region dipping at an angle of 60° between 25 and 65 km depth. She interpreted this as the subducting Cocos Plate. In agreement with this, and contrary to previous studies, a recent seismicity and tomography study of data from a local amphibious network in central Costa Rica [*Dinc*, 2008; *Dinc et al.*, 2010] does not find a significant shallowing of the subduction dip of the deeper part of the slab toward south Costa Rica. The cold and dense Cocos Plate is imaged as a high-velocity anomaly down to 70 km coincident with the WBZ seismicity, and overlain by a low-velocity layer.

3. Data Set: Talamanca Transect

[17] This study is based on the data by the Talamanca Transect, which was described in detail by *Dzierma et al.* [2010]. Sixteen Güralp broadband 3ESPD and 3TD seismometers were installed in

Table 1. Coordinates of the Talamanca Transect Stations Included in the Analysis and Number of Receiver Functions Analyzed per Station

Station Number	Station Name	Latitude	Longitude	Height (m)	Number of Receiver Functions
crt-02	Dominical	09°15.972	−83°51.547	0	68
crt-03	Tres Ríos	09°17.947	−83°48.311	415	23
crt-04	Alto San Juan	09°20.021	−83°44.131	828	76
crt-05	Miravalles	09°24.946	−83°40.747	1014	97
crt-06	San José de Rivas	09°26.687	−83°38.189	1205	48
crt-07	Los Ángeles	09°27.526	−83°35.095	1479	169
crt-08	Río Blanco	09°29.912	−83°36.733	1758	48
crt-11	Pejibaye	09°47.934	−83°41.906	728	113
crt-13	San Antonio Arriba	09°47.846	−83°33.74	1038	84
crt-14	Guineal	09°50.282	−83°31.743	955	184
crt-15	Moravia	09°48.878	−83°27.776	1223	159
crt-21	Río Orosi	09°46.376	−83°47.378	1572	165
crt-23	Jaular	09°39.682	−83°52.000	2398	123
crt-25	Alaska	09°31.279	−83°39.790	1585	170
crt-26	Cimarrones	10°04.777	−83°25.908	225	11
crt-27	Tres Equis	09°57.287	−83°33.645	613	113
crt-31	Guápiles	10°07.100	−83°48.650	700	44
crt-32	Guayabo Arriba	09°59.156	−83°43.228	1602	52
crt-33	La Esperanza	10°14.744	−83°56.036	1000	11
crt-34	Virgen del Socorro	10°16.020	−84°09.930	1642	19

spring 2005 along a transect through the northern Cordillera de Talamanca (Table 1 and Figure 2), close to the seismic profile by *Stavenhagen* [1998]. All stations operated for two years with a sampling rate of 100 Hz.

[18] A database of 322 teleseismic events was used for the receiver function analysis. Most of these were located either to the northwest (Alaska-Aleutian region) or to the southeast (Chilean subduction zone); a few events occurred at other back azimuths, and the inclusion of PP and PKP phases could further reduce the azimuthal gap (Figure A1 in section A1).

4. Method

4.1. Receiver Function Technique

[19] The receiver function technique makes use of the fact that part of the energy of seismic P waves is converted into S waves at discontinuities along the ray path. It belongs to the standard seismological methods for the investigation of crustal and mantle structure [e.g., *Vinnik*, 1977; *Owens et al.*, 1984; *Bostock and Rondenay*, 1999; *Jones and Phinney*, 1998; *Kind et al.*, 1995]. The main processing steps include rotation of the recorded seismogram components into the ray coordinate system (L, Q, T) and water level deconvolution with the L trace containing the P wave signal. The single-trace receiver functions are made comparable to each other by correcting for the effect of ray parameter on the conversion delay time, referred to as normal moveout correction (NMO). A detailed outline of the data analysis is given by *Dzierma* [2009] and *Dzierma et al.* [2010].

4.2. Quality Control, Ray Coverage, and Resolution

[20] The signal-to-noise ratio (SNR) on the L component was calculated and traces with low SNR (1.4–2) were visually quality checked. Only those traces were included in the analysis where a good P onset could be discerned, giving a total of 1777 receiver functions.

[21] The ray coverage can be illustrated by plotting the piercing points (Figure 3), that is, the locations where the rays pierce a given depth plane. Due to the spread-out of the rays under each station, the latitudinal coverage increases with depth and piercing points from different stations overlap.

[22] To retrieve the deep structure (sub-Moho depths) of the Costa Rican land bridge, the receiver functions are filtered with a low pass of corner frequency 0.2 Hz; this is necessary to suppress high-frequency noise. The filtering limits the vertical resolution (about half an S wavelength [*Bostock*, 1999]) to about 25 km in the mantle. The horizontal resolution (the first Fresnel zone) in the mantle is about 30 km.

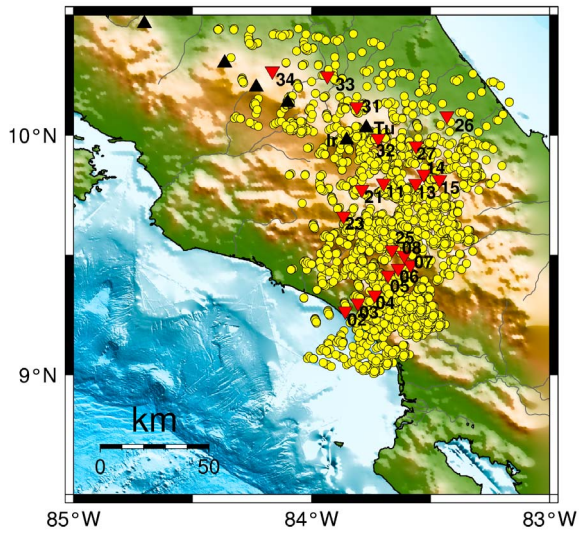

Figure 3. Piercing points for the Talamanca transect stations at 50 km depth (yellow).

[23] The stability and accuracy of the observations is checked by a bootstrap test [*Efron and Tibshirani*, 1986], in which the analysis is performed for two independent data subsets (odd-numbered versus even-numbered traces) and the results are compared to determine which features are stably reproduced (Appendix A).

4.3. Imaging Method

[24] In the presence of dipping structure or anisotropy, the arrival time and polarity of the receiver functions depends on the back azimuth, which means that traces from different back azimuth cannot be stacked. The results by *Dzierma et al.* [2010] have shown that this azimuthal problem exists for this data set, so stacked traces will not be considered in the present study. The interpretation of the individual traces is complicated particularly in this setting, where dipping structures (the slab) may be expected and anisotropy has been observed [*Hoernle et al.*, 2008; *Abt et al.*, 2009].

[25] Prestack migration algorithms exist which can be applied in the presence of 2-D and 3-D structure if these have been sampled spatially dense enough in terms of receiver coverage and seismic source distribution [*Bostock et al.*, 2001; *Shragge et al.*, 2001; *Rondenay et al.*, 2001; *MacKenzie et al.*, 2010]. For logistical reasons the Talamanca transect had to be sampled along a crooked line with irregular spacing. As station spacing was not sufficiently dense, prestack migration could not be applied successfully. Instead, we applied the more robust standard back projection algorithm for imaging the crustal and upper mantle structure, which uses ray tracing and a 1-D approximation of the seismic velocity model to transfer the receiver functions from the time to space domain [*Dzierma et al.*, 2010; *Gossler et al.*, 1999; *Jones and Phinney*, 1998; *Yamauchi et al.*, 2003; *Yuan et al.*, 2000]. Each ray is traced back into the subsurface, so that each recorded sample (with its conversion amplitude) can be associated with a location. The subsurface volume is gridded, and the amplitude in each grid cell is determined as the weighted sum of the amplitudes of the traversing rays. The resulting volume of conversion amplitudes is projected onto a profile through the transect and smoothed with a moving filter of width 20 km (Figure 4).

[26] This imaging technique is generally applied based on a 1-D velocity model (although the rays are traced in a 3-D volume), which usually gives reasonable results [e.g., *Dzierma et al.*, 2010; *Gossler et al.*, 1999; *Kosarev et al.*, 1999; *Ramesh et al.*, 2005; *Yuan et al.*, 2000]. A different choice in velocity model will only shift the signals by a few kilometers, usually less than the vertical resolution achieved by the receiver functions. We use the available 1-D regional velocity model for Costa Rica by *Quintero and Kissling* [2001]. Although some limitation on the accuracy of the image is posed by the fact that a 1-D velocity model underlies the ray tracing, we interpret the results by comparison with the modeling study, where imaging is performed in exactly the same way.

5. Results

5.1. Imaged Profile

[27] The most conspicuous feature observed in the deep structure (Figure 4) is a strong positive conversion dipping toward the northeast with a steep angle of about 65° down to a depth of about 170 km. The velocity contrast that causes the dipping conversion is preliminarily interpreted as the subducting slab. This creates two signals, a negative conversion attributed to the low-velocity subducting crust followed by a positive conversion at the high-velocity slab mantle. Even when both signals are broadened by filtering, the zero crossing between them remains approximately stable.

[28] Because of the low-pass filtering, the shallow structure of the overriding plate is not well resolved. Thus, the Moho and crustal structure are merged together into a pronounced positive signal

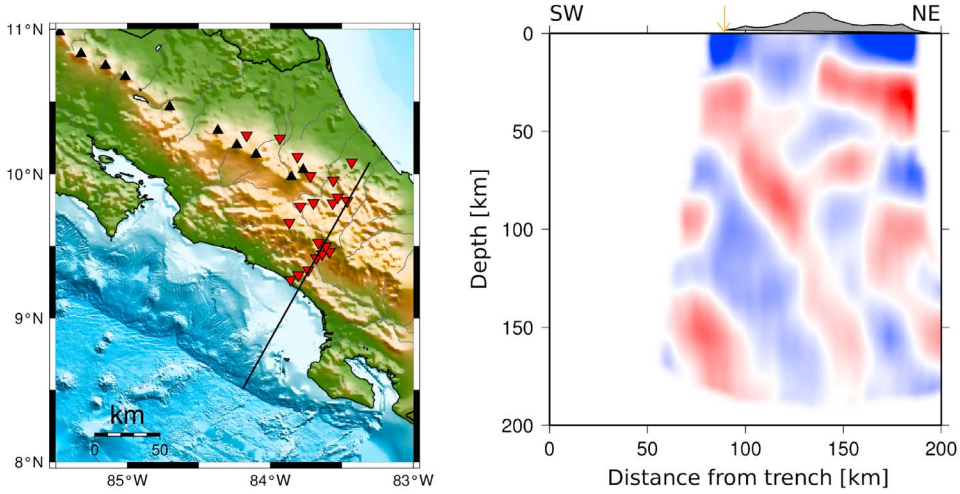

Figure 4. Trench-normal receiver function profile through the migration volume. (left) Map of receiver function profile. The profile starts approximately at the trench and trends normal to the trench (about N30°E) for 200 km. (right) Imaged receiver function profile. Receiver functions were low-passed below 0.2 Hz before migration, and the migrated section was then smoothed with a 20 km Gaussian filter for plotting. Red amplitudes denote positive conversions, and blue amplitudes denote negative conversions. Depth and distance from the trench are both in km (to scale). The topography is overlain in grey, with amplification factor 4, and the coastline is indicated by an arrow.

at 30–40 km depth. Moho multiples are seen at around 100 km depth at the outer edges of the profiles. The positive conversions dipping steeply around 150–200 km depth in the southwest of the profiles correspond to slab multiples (see forward modeling studies below).

[29] The bootstrap test (Figure A2 in Appendix A) confirms the major features identified in the imaged profile, and deviations in the depth of converted signals are smaller than the depth resolution.

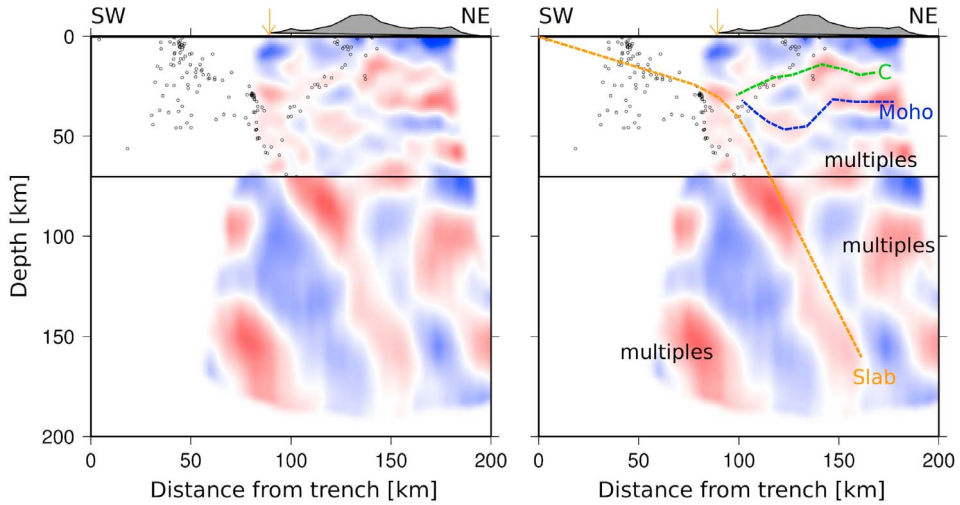

Figure 5. Trench-normal receiver function profile through the migration volume. (left) Low-frequency profile with high-frequency shallow structure and seismicity overlain. The deep profile corresponds to the one shown in Figure 4, and the shallow profile was analyzed by *Dzierma et al.* [2010]. It was processed and migrated in the same way but filtered with a 1 s low pass and a Gaussian of filter width 7 km. Seismicity recorded by the Quepos network [*Dinc et al.*, 2010] is overlain on the shallow structure. (right) Interpretation of the main features. The slab close to the trench is assumed to dip at an angle of 18°. At depth, a dip angle of about 65° is observed. The interpretation of the shallow features (the crustal interface C and the Moho) is similar to *Dzierma et al.* [2010].

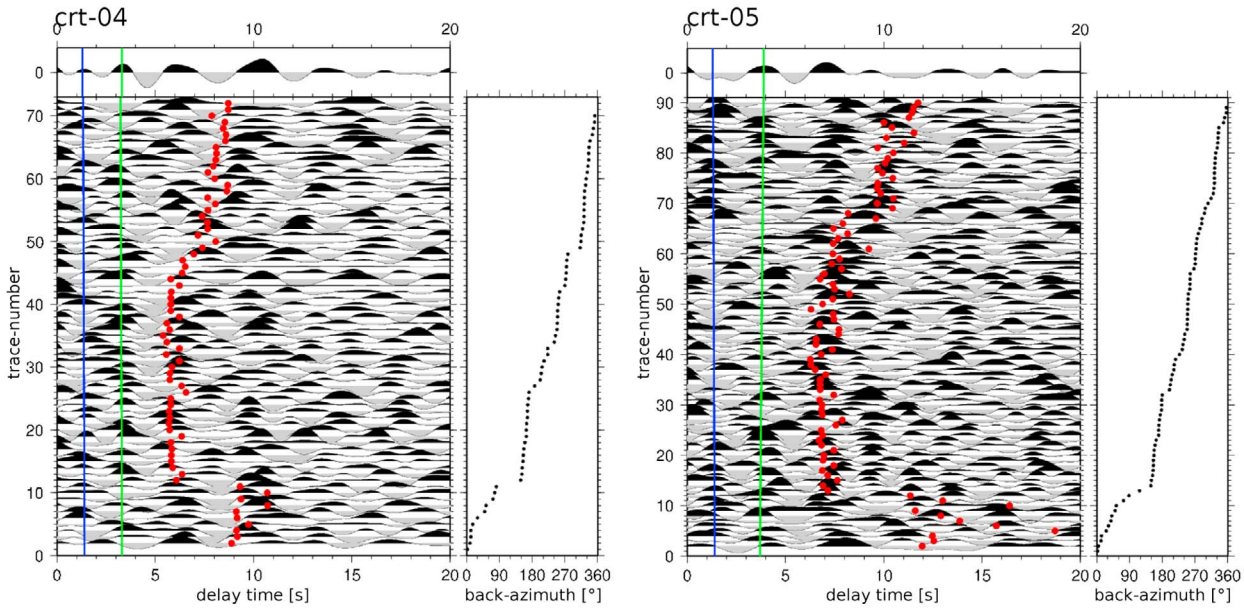

Figure 6. Radial receiver functions (individual traces) for stations (a and b) crt-04 and (c and d) crt-05. The traces were filtered with a 2 s low pass and sorted by back azimuth (Figures 6b and 6d). The green line marks the Moho arrival, which is clear in the single traces and is also well reflected in the stacked section (shown at the top of Figures 6a and 6c). The blue line marks the preceding crustal discontinuity. Although this arrival is somewhat disrupted in some back azimuth ranges, it is still sufficiently coherent to stand out as a clear conversion and also appear in the stacked trace. The red dots mark the expected delay times of a slab signal created by a 57.5° dipping slab at 56 km depth below station crt-04. For crt-05, the expected slab signal times were calculated for a 60° dipping slab at 72 km depth. Some scatter in the times is caused by different epicentral distances.

[30] To allow for the interpretation of the crustal structure, the higher-frequency recordings by *Dzierma et al.* [2010] are overlain in Figure 5, together with the seismicity recorded by the Quepos network (Figure 2) [*Dinc et al.*, 2010] and an annotated version with the proposed preliminary interpretation. In the combined image, the position of the subducting slab close to the trench is estimated based on the recorded seismicity and the known slab dip of about 18° down to about 30 km depth [*DeShon et al.*, 2003; *Stavenhagen et al.*, 1998]. Near the coastline, the seismicity meets a positive dipping conversion which appears to bend toward steeper dip, and which was tentatively interpreted as a subducting slab signal by *Dzierma et al.* [2010]. This interpretation agrees with the position of the signal interpreted as a dipping slab in the low-frequency receiver functions. It has been observed in many subduction zones that an initial shallow slab dip of 15°–20° gives over to steeper subduction angles at a similar depth (this is also observed in central and north Costa Rica by *Protti et al.* [1995]), so we believe this interpretation is plausible.

[31] Given the fact that receiver function analyses were originally developed for near-horizontal structures, we must make sure if the observed dip is consistent with the signal in the individual traces. Since the imaging method has some shortcomings when applied to dipping structures, we will also check by forward modeling whether a steeply dipping slab would really be visible in the image sections, and if the observed signal could be created in the absence of a dipping slab, e.g., by an underplating scenario.

5.2. Dipping Structure Effects in Individual Traces

[32] The effects of the proposed steeply dipping slab on the individual traces are complicated, in particular since the azimuthal coverage is not uniform. In addition to an expected sinusoidal variation of conversion arrival times, additional anisotropy effects may be present [*Cassidy*, 1992; *Savage*, 1998; *Schlindwein*, 2001]. These effects and the arrival of crustal multiples and slab conversions at similar times make a direct intuitive interpretation difficult.

[33] Close to the coast, the slab is very shallow and the signal cannot easily be distinguished from the crust of the upper plate. We therefore consider stations with more than 100 km distance from the trench, starting with crt-04 (Figures 6a and 6b). Assuming a slab depth of 56 km below crt-04 and a dip of 57.5°, the piercing points where the rays would intersect the slab are calculated based on backward ray tracing. The corresponding delay times are plotted in the azimuthally sorted trace gather (nmo corrected). In addition to coherent arrivals from the Moho (at around 3.3 s) and from the crustal discontinuity (about 1.4 s), the predicted slab conversion times can be observed close to a marked negative-positive bimodal conversion. This is the kind of signal expected for a subducting slab, if a low-velocity layer overlies a higher-velocity slab. While these conversions can hardly be recognized in the single traces without the synthetic calculations to guide the eye, the feature is rather clear when compared with the expectations. Although there are also positive conversions at different times (e.g., back azimuth 0–90° and 330–360° at 6–7 s), these are not preceded by negative-polarity conversions and are therefore not identified as a slab conversion. The positive signal at this time is probably a multiple of the crustal structure. In the same way, the Moho multiple around 11 s delay time can also be distinguished from the slab signal.

[34] Similarly, the slab conversion at station crt-05 can be approximated with a dip angle of 60° and a depth of 72 km (Figures 6c and 6d). If the slab is indeed at 56 km depth below crt-04 (at a distance of about 105 km from the trench) and at 72 km depth below crt-05 (distance 115 km from the trench), it would dip at an angle of about 58°, in agreement with the dip estimated below the stations.

[35] The simple forward calculation of expected slab arrivals gives good results for most stations with a large number of traces from different back azimuths (crt-04, crt-05, crt-06, crt-07, crt-08, crt-13, crt-14, crt-15, crt-21, crt-23, crt-25, crt-27), which gives an impression that the proposed dipping geometry is broadly consistent with the individual traces. However, the occurrence of multiples and the azimuthal effects make a reliable interpretation of the individual traces difficult, and some ambiguity in the results cannot be avoided at several stations. For example, the signal observed at crt-07 could be fit equally well for any slab dip between 60° and 80° (Figure A3 in Appendix A), as long as the slab depth is about 88 km below the station. This depth is retrieved stably because of the strong conversion signal observed at early times (for back azimuth around 180°), but in the downdip direction it cannot be decided which conversion represents the slab signal. For these traces, more sophisticated models are required, which are presented below.

5.3. Forward Modeling

[36] The resolution of the upper mantle structure along the Talamanca transect shows some limitations caused basically by three factors: low signal frequencies, limited profile length and image distortions possibly caused by the back projection approach. For example, laterally heterogeneous structures, such as edges and flexures, can create scattered arrivals which can show similar travel times or dips as arrivals from steeply dipping interfaces [*Morozov*, 2004; *Morozov and Zheng*, 2006]. However, these and other structures can be distinguished from each other up to a certain degree if the seismogram sections are considered in terms of amplitude and waveform, too. Therefore, we defined a number of hypothetical subsurface models and computed synthetic receiver function images which can then be compared to the field data in order to rule out inadequate models and to get better insight into the structural resolution. For the modeling we applied the 2-D finite difference code FDMPI of *Bohlen* [2002] (details in section A2).

[37] For all models, the slab starts at the trench with a subduction angle of 18°, since this is well constrained [e.g., *Stavenhagen et al.*, 1998]. From a depth of about 35 km onward (under the coastline), the continuation of the slab is unclear, so different models explore the possible geometries of the slab at depths >35 km. The tectonic scenarios coming into consideration are the following: (1) a steeply dipping slab, (2) slab break-off at depth, and (3) slab underplating or shallow angle underthrusting.

[38] Common to these models are the following P and S wave velocities (v_p, v_s) and densities ρ: (1) upper crust (overriding plate), v_p = 5.8 km/s, v_s = 3.2 km/s, ρ = 2.0 kg/l; (2) lower crust (overriding plate), v_p = 6.8 km/s, v_s = 3.9 km/s, ρ = 2.6 kg/l; (3) mantle wedge, v_p = 7.6 km/s, v_s = 4.343 km/s, ρ = 3.4 kg/l; (4) subducting slab, v_p = 8.0 km/s, v_s = 4.57 km/s, ρ = 3.5 kg/l; (5) low-velocity layer on top of subducting slab (8 km thick), v_p = 6.5 km/s, v_s = 3.757 km/s, ρ = 2.65 kg/l; and (6) trench (prism-shaped), v_p = 3.0 km/s, v_s = 1.714 km/s, ρ = 2.0 kg/l. The choice of the

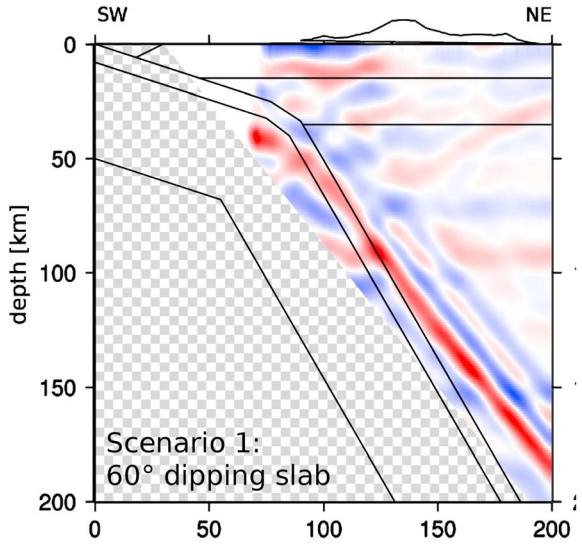

Figure 7. Finite difference model results for a model with a 60° dipping slab. The basic model geometry is overlain as black lines. The reflection of the incoming plane wave at the model boundaries creates a group of later arriving waves coming from the side, which is shaded in the results.

velocities was made to represent average upper and lower crustal velocities similar to those determined by *Stavenhagen* [1998]. We included a low-velocity crustal layer on top of the subducting slab, since the single-trace receiver functions point to a negative-positive conversion. We assume the presence of a low-velocity crustal layer on the slab is realistic, since this has also been observed in many subduction zones [e.g., *Abers*, 2005]; its inclusion or omission from the model does not change the main structure of the results, although it slightly enhances the visibility of the dipping conversion. The relatively low velocity in the mantle wedge was chosen with serpentinization in mind, which had been observed in northern Costa Rica [*Grevemeyer et al.*, 2007; *Dinc*, 2008; *Ivandic et al.*, 2008]. While for central and southern Costa Rica, such a high serpentinization value (about 15%) may be unrealistic, this does not considerably influence the results as long as the velocity contrasts at the discontinuities are adequate. Receiver function amplitudes are sensitive mainly to the change S velocity at an interface; the assumed velocity contrast of 6% at the slab relative to the mantle wedge corresponds to the generally observed values for subduction zones worldwide (compare, e.g., *Helffrich* [1995]). v_p/v_s is assumed to be 1.75 in the whole model. The models considered here were designed to test simple scenarios that might be expected for the subduction zone. They were not optimized for the best fit to the individual traces, where the thickness of the crust, depth of the slab, velocities and v_p/v_s ratio should be determined with accuracy. The aim of this modeling study is rather to check different proposed scenarios for subduction/underplating and compare them with the observed receiver function image.

[39] We would like to emphasize that the imaging algorithm applied to the modeled traces is the same as for the field data, the only difference is that the incoming rays are all in the plane of the model. Any misimaging introduced by ray tracing based on a 1-D model is the same as would occur for the field data, so that the results from the modeling study are comparable to the observed data set.

[40] All the results are plotted with the same amplitude scale for comparability. Although the Moho and crustal interface and velocities are kept the same for all models below, some variation in Moho and inner crustal conversion amplitudes is still observed. This is due to the fact that the ray paths are influenced by the underlying structure, which is different for all models. If the rays meet an inclined surface, they are refracted and therefore their angle of incidence on the horizontal Moho and crustal structure changes. Since the conversion amplitude is dependent on the angle of incidence, the conversion amplitude of the Moho and crustal interface, together with their multiples, is different for the models. Where the rays strike the Moho at near-vertical incidence, the conversion amplitudes will be very small and the horizontal structures near invisible. In the extreme case, the continental Moho may even produce a negative conversion if the model geometry is such that the velocity structure is inverted: when the slab low-velocity zone directly underlies the continental Moho, this will produce a negative conversion rather than the usual positive Moho conversion when the velocities increase from the crust into the mantle wedge.

5.3.1. Scenario 1: 60° Dipping Slab

[41] We start with a simplified model based on the observations. Here, the slab bends underneath the coastal stations to steep subduction at an angle of 60° (below about 40 km).

[42] The dipping slab is evident in the resulting model section (Figure 7). The slab is retrieved well, with an angle close to the input dip angle and at approximately the correct position. The crustal interface and Moho conversions are imaged at the

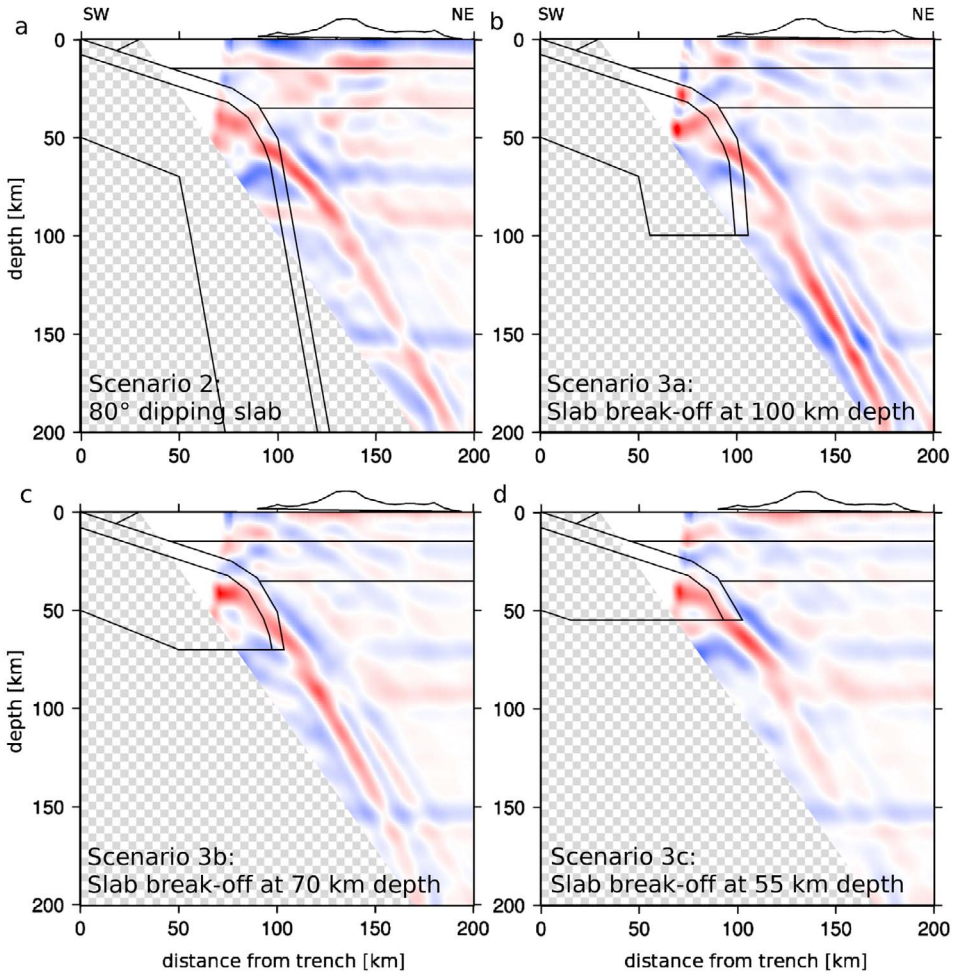

Figure 8. Finite difference model results for various models with an 80° dipping slab, as discussed in the text.

correct depth. The multiples occur at depths of about 60 km (crustal interface) and 100 km (Moho), in good agreement with the observations. In total, the interpreted structure from Figure 4 (crustal and Moho conversions, multiples, and dipping slab signal close to the coast) is reproduced. However, the slab dip angle appears slightly shallower than in the input model (approximately 52° instead of 60°), and the slab is observed somewhat farther from the trench than it is. Therefore, the modeling is repeated for a steeper input dip angle.

5.3.2. Scenario 2: 80° Dipping Slab

[43] If an input dip angle of 80° below 40 km depth is modeled, the retrieved profile indeed shows a steeply dipping slab signal with an apparent angle of 60° in the image section (Figure 8a). The slab conversion is clearly imaged, although the dip angle is underestimated. The crustal and Moho signal are clearly visible at the correct depth.

5.3.3. Scenario 3: Slab Break-Off at Depth

[44] If the slab is torn off at depth, the dipping signal is artificially prolonged by a scattering hyperbola originating at the slab edge. To show this effect, we calculated models with a slab break-off at 100 km (scenario 3a in Figure 8b) and 70 km depth (scenario 3b in Figure 8c). The dipping signal persists even where the slab is no longer present, although it fades out eventually at large distances. The slab break-off modeled in this scenario is very sharp and with extremely abrupt slab edges, which causes strong scattering signals that may be unrealistic; but it shows that it is impossible to determine exactly where the slab ends. However, for an extremely shallow slab break-off, the

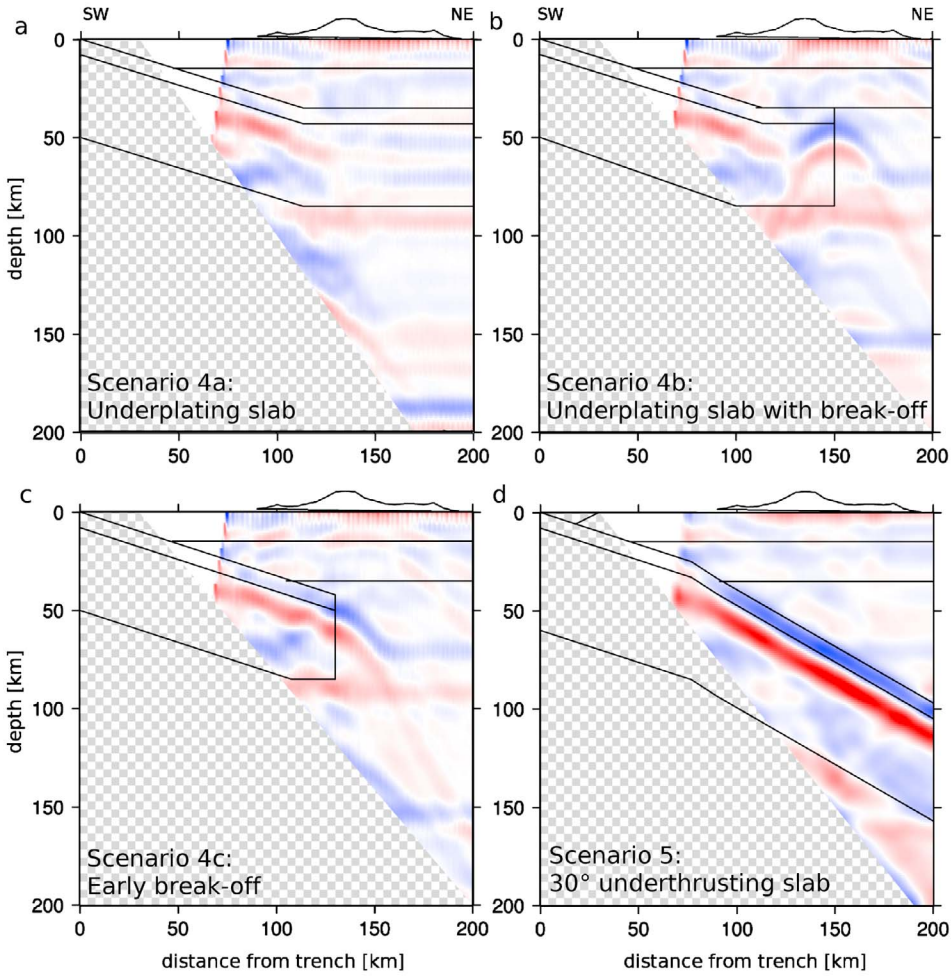

Figure 9. Finite difference model results for various models with a shallow underthrusting slab, as discussed in the text.

amplitudes would be expected to fade out, which is not observed. Moreover, the crustal and Moho signal in the break-off scenario are significantly weaker, in contrast to what is actually observed. A similar effect is seen when break-off occurs even earlier, at 55 km depth (the transition between 60° and 80° dip in our models). Again, it is clear that some kind of dipping signal is created if slab break-off occurs at the right point (Figure 8d). However, even though this model clearly has unrealistically large scattering amplitudes because the tip of the slab is so abruptly cut off, the fade-out of the scattering signal is even more pronounced in this scenario, and the Moho and crustal signal are not retrieved clearly. It is unlikely that this very exaggerated geometry should occur in just the right way and just the right place to produce the observed signal. We therefore believe that a slab break-off shallower than at least 70 km is not plausible, and that the Cocos Plate should subduct to depths of the order of about 70–100 km or more.

[45] All our models include a bend or kink in the slab at the transition from the shallow subduction at about 18° toward steeper dip angles. To make sure that the modeling results are not markedly influenced by scattering produced at the slab bend, we investigated models with continuously steep dips of 60° and 80° (Figure A6). In both models, the dipping slab is imaged clearly and with angles similar to those presented in the dipping slab scenarios 1 and 2 above (see section A3 for full discussion).

5.3.4. Scenario 4: Underplating Slab

[46] To test if a dipping slab needs to be present at all, an underplating fast slab is modeled (scenario 4a in Figure 9a). This is assumed to bend abruptly at 35 km depth, underplating directly

below the overriding plate Moho. Apart from the dipping conversions caused where the slab descends under the overriding plate, the underplating slab can hardly be discerned in the receiver functions. This is expected for the ray geometry (close to the vertical); it is evident that this scenario cannot create the observed dipping signal.

[47] Assuming that an underplating slab were broken off close to the center of the seismometer transect at about 150 km distance from the trench (scenario 4b in Figure 9b), a scattering hyperbola is created with the apex under the station where the slab terminates. Still, this scattering signal could not be confused with a dipping signal unless the break-off occurs right at the end of the dipping part of the slab, similar to scenarios 3b and 3c in Figures 8c and 8d.

[48] In an attempt to recreate the observed dipping signal just by slab break-off, the above model is refined so that the slab break-off occurs even more shallow: in this model (scenario 4c), the slab subducts at an angle of 18° to a depth of about 40 km (around 130 km distance from the trench) and then breaks off abruptly (Figure 9c). The extreme geometry of the slab edge causes a scattering hyperbola that may be unrealistically strong. Even so, the dipping signal created by scattering has much smaller amplitude than what is observed in the data. While the bending part of the scattering hyperbola is still clearly visible, the near-straight dipping signal is extremely weak and would not easily be confused with a dipping signal. Besides, the scattering signal is placed much farther from the trench than what is observed in the data. To obtain a dipping signal at the observed position, slab break-off would need to occur at about 70 km distance from the trench and at very shallow depths of about 30–40 km; at this position, the slab is still seen clearly in tomography images [*Dinc et al.*, 2010], so this scenario is not realistic.

5.3.5. Scenario 5: 30° Dipping Slab

[49] Finally, we check the proposed scenario that the slab might underthrust at a shallow angle. For this, we assume a subduction angle of 30° underneath 40 km depth (scenario 5 in Figure 9d). The subduction angle in this model is exactly imaged, which is in disagreement with the observations.

5.3.6. Summary of Modeling Results

[50] Based on the comparison of the input model geometry with the observed dipping signal, we can now offer a summary interpretation for the slab geometry. All our models needed at least a steeply dipping (~80°) slab down to depths of 70–100 km to create conversions similar to the observed signal. The dipping slab is located somewhat closer to the trench than in the preliminary interpretation offered above (Figure 5), which agrees better with the seismicity. Supposing that the velocity contrast that is imaged in the receiver functions is the subducting plate Moho, this would explain why the seismicity is slightly above the slab conversion.

[51] We are aware that the deeper part of the dipping slab signal may be caused by scattering after slab break-off; this cannot be decided based on the present data set. However, it has not been possible to simulate a dipping signal for a scenario of shallow angle underthrusting or underplating. All the models had to rely on at least a minimum length of several tens of kilometers of steeply subducting slab to create dipping conversions.

6. Discussion

6.1. Along-Arc Variations

[52] To check whether along-arc variations in the geometry can be observed in the data, we image four parallel profiles all trending normal to the trench (Figure 10). In this case, only a stripe of 20 km width to either side is projected onto the profiles.

[53] Except for some lateral variation in the shallow structure (discussed by *Dzierma et al.* [2010]), the deeper structure is similar in all the profiles. In particular, a lateral change in slab dip angle is not apparent. In comparison with the combined profile, the slab signal in the narrow-width profiles is not as pronounced. At 120–130 km depth, the positive conversion is thinned and in some profiles interrupted, but reappears again about 10 km deeper. This interruption occurs at a similar depth where the crustal multiples would be observed; they are again visible at the outer edges of the profiles. Below the distortion, the slab signal can be followed to depths of 160–170 km except in the southern profile (4), where ray coverage is poor and no clear signal can be seen below 150 km depth.

[54] We believe that the thinning of the slab signal at depth may be a combined effect of the multiples and the observation geometry. Some weakening of the slab signal is also evident in the forward modeling scenarios. Since fewer traces are avail-

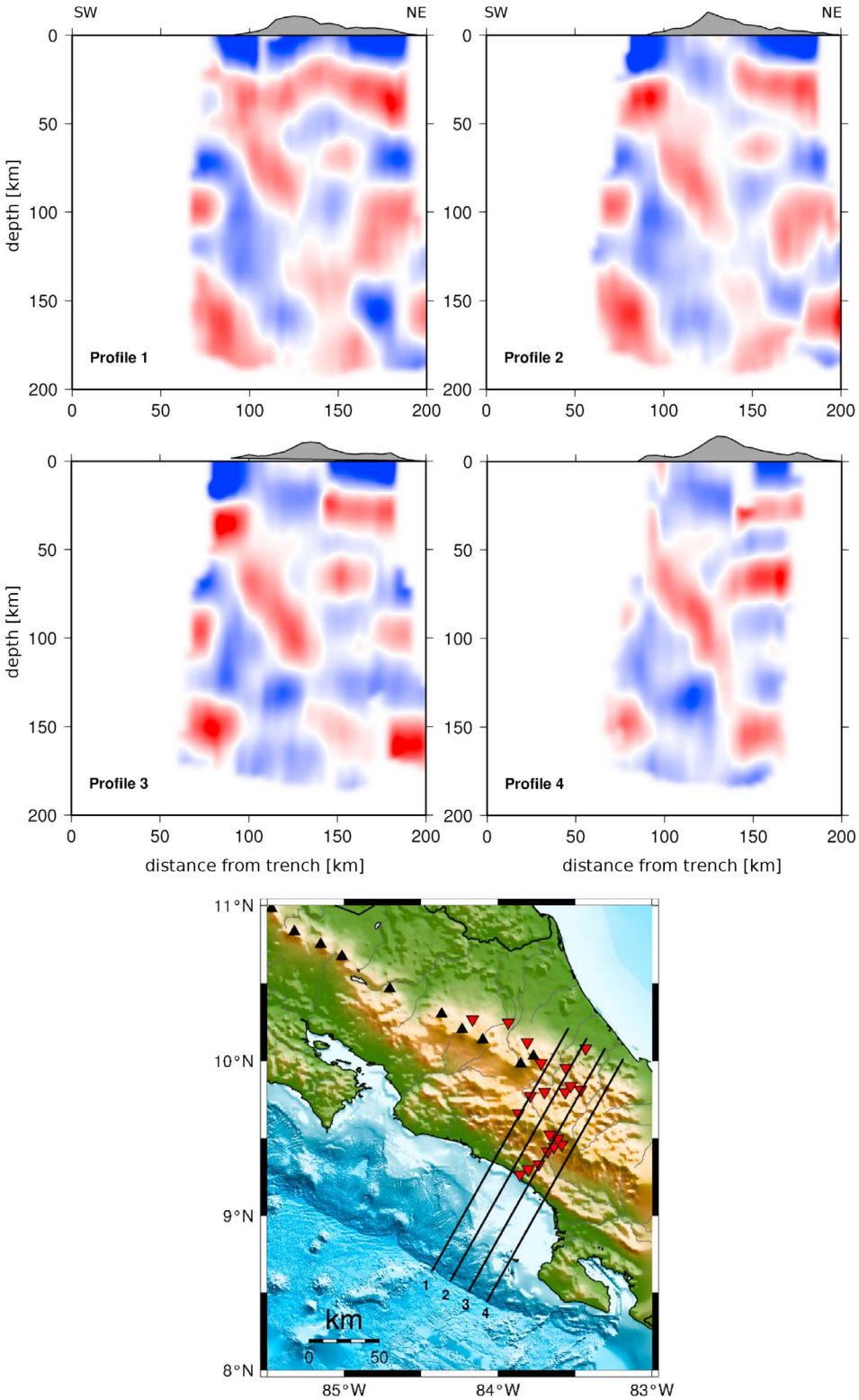

Figure 10. Low-frequency trench-normal receiver function profiles through the migration volume. A strip of 20 km width has been projected onto these profiles so that lateral variations in structure are resolved. The positions of the profiles are shown on the map. All profiles start at the trench (km 0) and trend normal to the trench (about N30°E) for 200 km. The spacing between the profiles is 45 km.

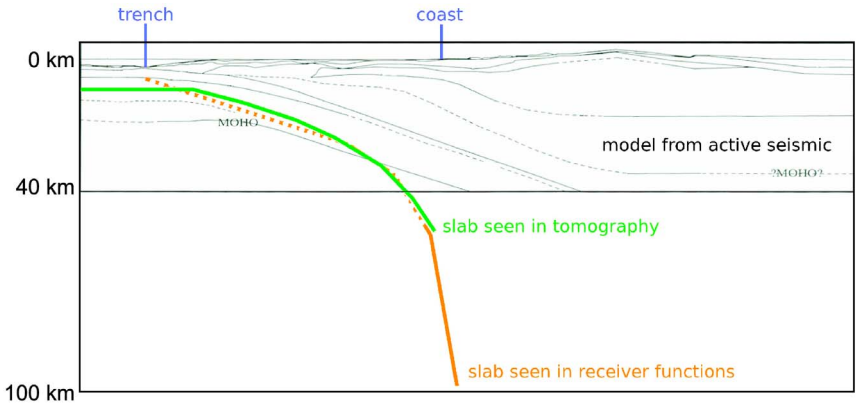

Figure 11. Schematic comparison of the slab seen in active seismic profile from *Stavenhagen* [1998] (black line) with the tomography result by *Dinc* [2008] (green line) and with the receiver function–based interpretation (orange line). The position of the slab from tomography was picked by Dinc to obtain a surface, the southern edge of which is shown here (slightly smoothed).

able when the profiles are restricted to narrower stripes, phase changes and back azimuth effects can play a greater role in disturbing the signal. The fact that the slab signal is retrieved stably in the bootstrap tests affirms its credibility. Apart from the gap in the slab signal, all the main features of the total profile (Figure 4) are retrieved in the thin profiles, giving an independent confirmation of the stability of the results. At the same time, this shows that no significant lateral changes can be observed in the deep structure over the width of the volume investigated here (spanning about 150 km along-arc distance), given the resolution of the data set.

6.2. Comparison With Previous Studies

[55] We compare the proposed interpretation of the steeply subducting slab with results from local earthquake tomography by *Dinc et al.* [2010] and from active seismic by *Stavenhagen* [1998] (Figure 11). The slab position from tomography was determined by *Dinc* [2008] by visually picking the interpreted slab surface in the tomography sections; we have here used the southernmost edge of the slab surface for the comparison. The slab from receiver functions is based on the comparison of the forward modeling with the observations; it is plotted as a solid line where it is confirmed by observations and dotted following the input model. The proposed slab we observe agrees well with the position of the slab from local earthquake tomography and with active seismic. At shallower depths the tomography results compare well with the active seismic results from *Stavenhagen* [1998], perfectly matching the shallow dip close to the trench, but then bending toward steeper subduction below the depth range imaged by active seismic. The tomography study clearly shows the transition from shallow dip (18°) to steeper dip and hence links the receiver function image with active seismic studies. The receiver functions image the continuation of the steeply dipping regime of the slab down to far greater depths. Combining these three methods, the complete picture emerges and the subducting Cocos Plate is imaged from the trench down to very steep dips, which occur at depths in excess of about 70 km.

[56] Along the northern boundary of the study region, the imaged slab is also consistent with the seismicity observed by *Protti et al.* [1994, 1995] and *Quintero and Kissling* [2001]. Further south, their seismicity diminishes rapidly. In contrast, data from a temporary network installed in the far south of Costa Rica indicates a poorly defined but steeply dipping (60°) seismic plane beneath Osa Peninsula [*Arroyo*, 2001]. Our study does not extend so far south; but it can estimate the geometry beneath the northern edge of the Talamanca, which is already influenced by the subduction of the transition between the seamount segment and the Cocos Ridge flank.

[57] The changes between the different profiles are very slight. If we accept that the dipping structure in the northern profiles corresponds to the subducting Cocos Plate in agreement with tomography and seismicity, we see no reason to interpret it as anything different in the south. Thus we believe it is plausible to assume steep subduction is imaged

under the whole study region in south-central Costa Rica, with no marked change in subduction angle toward the south.

[58] A hypothetical slab window formed by slab break-off or ridge subduction as proposed by *Johnston and Thorkelson* [1997] and *Abratis* [1998] would be under the northern edge of the area imaged by receiver functions (Figure A7 in section A4). The receiver functions cannot decide whether or not such a slab window exists; what this study shows is only that the slab window cannot start before the slab has reached 70–100 km depth.

6.3. Implications for Cocos Ridge Subduction

[59] Given the tectonic setting close to the edge of the Cocos Plate, it is likely that steep northeast trending subduction should cease close to the Costa Rican–Panama border. Whether the subduction zone approaching this boundary from the north will shallow or just continue steeply to the close vicinity of the slab edge has been debated. The receiver functions show no shallowing along the northern flank of the Cordillera de Talamanca yet, at a distance of 50–100 km from the landward projection of the PFZ. The slab dip imaged along the onshore projection of the seamount segment and Cocos Ridge flank remains virtually the same in the study area, with a steep dip of about 80° below 50 km depth.

[60] Since the study region is only about 50 km to the north of the Cocos Ridge crest, we believe it is unlikely that the ridge crest should underplate or underthrust at a very shallow angle below 50 km depth. Since the incoming oceanic crust offshore profile 4 is already thickened to about 12 km [*Sallarès et al.*, 2003; *Stavenhagen*, 1998; *Walther*, 2003], it is improbable that the plate should bend so strongly or tear through the thick crust without showing significant tectonic effects such as a fracture zone in the brittle part of the lithosphere.

[61] The generally accepted model is that aseismic ridges are buoyant features which resist subduction [e.g., *Vogt*, 1973; *Pilger*, 1981; *Nur and Ben-Avraham*, 1983; *Gutscher et al.*, 2000; *Yañez et al.*, 2001; *Pardo et al.*, 2002] with only few exceptions [e.g., *Tassara et al.*, 2006; *Guillier et al.*, 2001]. If we observe steep subduction of the southern Cocos Plate below 50 km, a possible explanation may be that only a short length of the Cocos Ridge has been subducted up to now (up to 100 km as proposed by *Stavenhagen* [1998]). In this case, the buoyancy would not yet be strong enough to counteract the still active slab pull on the subducted part of the slab. The most plausible scenario would then be one of moderately shallow angle subduction along the subducted part of the Cocos Ridge, giving over to steep subduction underneath.

[62] Based on analogue modeling, *Espurt et al.* [2008] have argued that the subduction geometry after the onset of plateau/ridge subduction remains unchanged until about 360 km of the plateau have been subducted, corresponding to about 7 Ma. During plateau/ridge subduction, the overriding plate shortens and uplifts above the termination of the flat slab. After about 10 Ma, shallow underthrusting is established. These predictions have been confirmed at several places (e.g., for the Nazca Ridge and Juan Fernández Ridge see *Hampel* [2002], *Rosenbaum et al.* [2005], *Yañez et al.* [2001], and *Ramos et al.* [2002]), even though realistic cases may also involve slab break-off [*Conrad et al.*, 2004]. It is still unknown when the Cocos Ridge arrived at the trench. The cessation of volcanism may indicate that the transition to shallow underthrusting is well underway, but it may not be completed yet. Possibly we are witnessing the phase of shallowing of the upper part and steepening of the lower part of the slab.

7. Conclusions

[63] We have presented a receiver function study along a transect of broadband seismometers through the northern Cordillera de Talamanca, which images a positive dipping conversion interpreted as the subducting Cocos Plate. The imaged slab agrees with previous results from local seismicity [*Dinc et al.*, 2010; *Protti et al.*, 1994, 1995; *Quintero and Kissling*, 2001], local earthquake tomography studies [*Dinc et al.*, 2010] and active seismic images [*Stavenhagen*, 1998], while extending the slab location to greater depths and steeper dip angle (up to 80°). The slab extends to at least 70–100 km depth. In this case, the emplacement of adakites in the Cordillera de Talamanca may not be linked with shallow underthrusting, but rather involve either the presence of a slab window [*Abratis and Wörner*, 2001] or the proposed mixing scenario by *Goss and Kay* [2006].

[64] Southward along the trench, no marked change is observed in the receiver functions. This suggests that the steeply dipping slab continues under the

northern flank of the Cordillera de Talamanca, opposite to the collision of thickened crust (>12 km) in the transition region between the seamount segment and Cocos Ridge. Although the study region does not extend far enough south to observe the deep geometry of the Cocos Ridge crest, the receiver functions suggest that steep subduction below 50 km is presently ongoing beneath the northern flank of the Cordillera de Talamanca, and might continue further south until the PFZ. A slight shallowing of the dip angle in agreement with slab stiffness is possible and may explain the observed arc-parallel mantle flow [*Hoernle et al.*, 2008; *Abt et al.*, 2009].

[65] We do not doubt that the shallow part of the slab is subducting at a shallow angle as a direct consequence of Cocos Ridge collision with the trench (compare, e.g., *Vannucchi et al.* [2006]). However, the deep structure below about 50 km does not show a shallow angle underthrusting slab. Here, the subduction appears to continue at a steep angle similar to northern and central Costa Rica [*Dinc et al.*, 2010; *MacKenzie et al.*, 2010]. This may indicate that only a short length of the Cocos Ridge has entered the subduction zone so far, which may cause the observed shallow underthrusting of the uppermost 30 km or so of the subduction zone geometry. As the establishment of shallow underthrusting is expected to take several million years after the onset of ridge collision [*Espurt et al.*, 2008], we may at present be witnessing a transitional phase in the development from steep subduction toward shallow angle underthrusting.

Appendix A

A1. Event Distribution and Quality Checks

[66] Figure A1 shows the azimuthal distribution of the analyzed receiver functions. Most events for which p phases were analyzed occurred in the southeast (Chilean subduction zone). Inclusion of pp phases could reduce the azimuthal gap, providing many events in the north (Alaska-Aleutian region) and west (east Pacific). There is a scarcity of events from the east, but other directions are well covered.

[67] To check the stability of the results, a bootstrap test was performed by analyzing the data subsets of even- versus odd-numbered events (Figure A2). The main features of the imaged profile are stably retrieved in both profiles.

[68] The azimuthal pattern of the receiver functions is consistent with dipping structure, the depth of which can be well constrained. The dip angle can be less clearly determined from the individual traces; for example, for station crt-07, dips between 60° and 80° can fit the observation well (Figure A3).

A2. FD Modeling

[69] The modeling is performed for a set of 81 receivers spaced equidistantly over a profile length of 200 km distance normal to the trench. For the applied program, it is impossible to consider rays coming from outside the model plane (trending normal to the trench at about N30°E). To realistically represent the distribution of incoming ray angles, we calculate the apparent angle of incidence of each observed ray after projection of the ray back azimuth and angle of incidence onto the model plane. Below the Moho, the incoming rays have theoretical angles of incidence in the range of about 10–30°. By projecting the ray paths onto the surface used for modeling, the apparent angle of incidence in the plane is reduced (Figure A4). In total, 44% of the rays come from the SW (the trenchward side of the model plane) at angles distributed around about 10°. Of those rays incoming from the NE (from the Caribbean direction), most have an angle of incidence around either 10° or 16–18° (17% have angles of incidence below 10°).

[70] As the different angles of incidence may result in different imaging effects, we consider the three most frequent angles of incidence in our modeling study (10°, 16° and −10°) and calculate a weighted average of the individual results. For each model run, the receiver functions are calculated and then back traced in the same way as was done for the field data set, projecting the conversion amplitude back along the ray path. As for the field data, the ray path is traced based on a 1-D velocity model, but propagating in the 2-D model surface. This creates a surface of conversion amplitudes which trends normal to the trench. The three surfaces for the different incidence angles are combined (weighted average). The resulting composite surface is then smoothed and plotted in the same way as the profile in Figure 4.

[71] The validity of combining the results for different angles of incidence is checked by comparing the modeling results for the different angles separately (Figure A5 shows an example for our preferred scenario; the results are comparable for all models). While some differences exist depending on the angle of incidence, the overall image is not

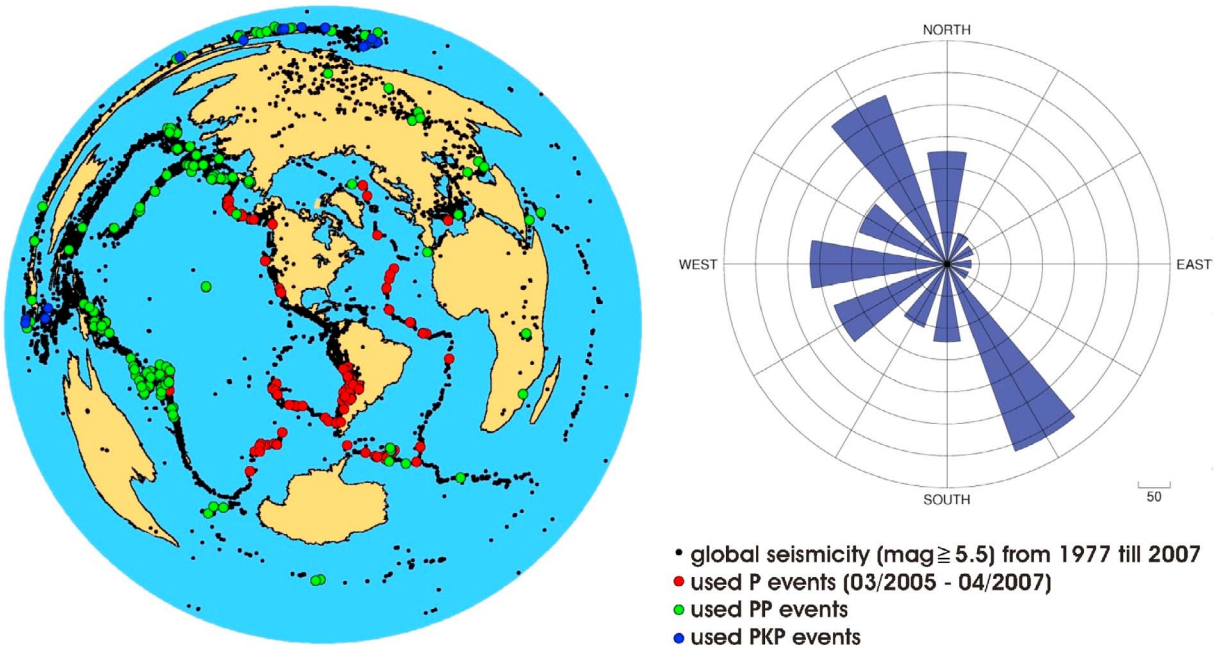

Figure A1. (left) Events used in the receiver function analysis. P phases are displayed in red, PP phases are in green, and PKP phases are in blue. For comparison, the global seismicity over a 30 year period is also plotted. (right) Azimuthal distribution of receiver function traces, plotted as a polar histogram.

changed markedly. In particular, the composite picture from summing the weighted contributions of the three scenarios again reproduces the input model sufficiently well. Slight displacements in the imaged slab position do occur, but are not dominant in the composite picture. For the models shown in the following, we only display the combined results, in all cases we have checked that the individual model outcomes give congruent results.

A3. FD Modeling With a Continuous Dipping Slab

[72] To test whether the bending or kink in the slab as it steepens has a disruptive influence on the modeling results, Figure A6 tests two different model scenarios. First, two models are calculated for a straight-dipping slab which has a constant angle from the surface to depth (60° and 80°). In

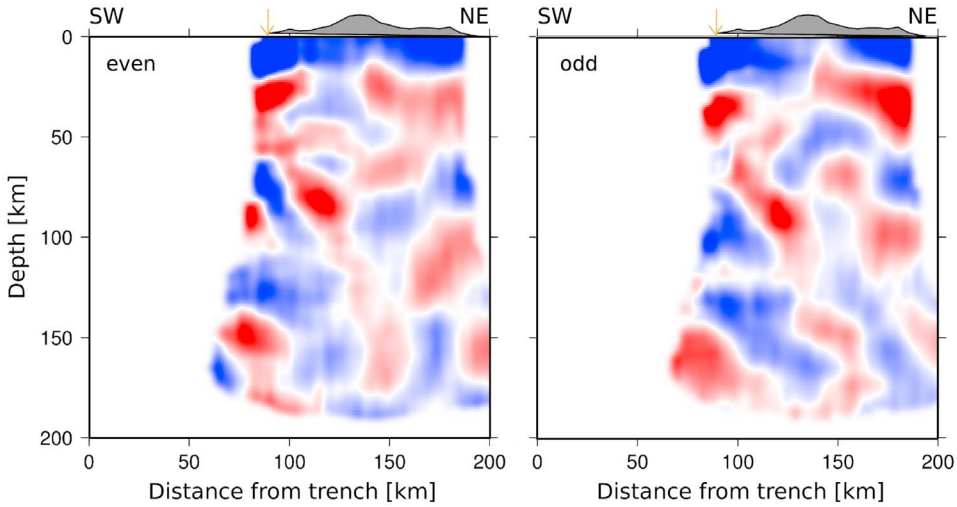

Figure A2. Bootstrap test for migrated receiver function profile. (left) Migration using even-numbered traces only and (right) migration using odd-numbered traces.

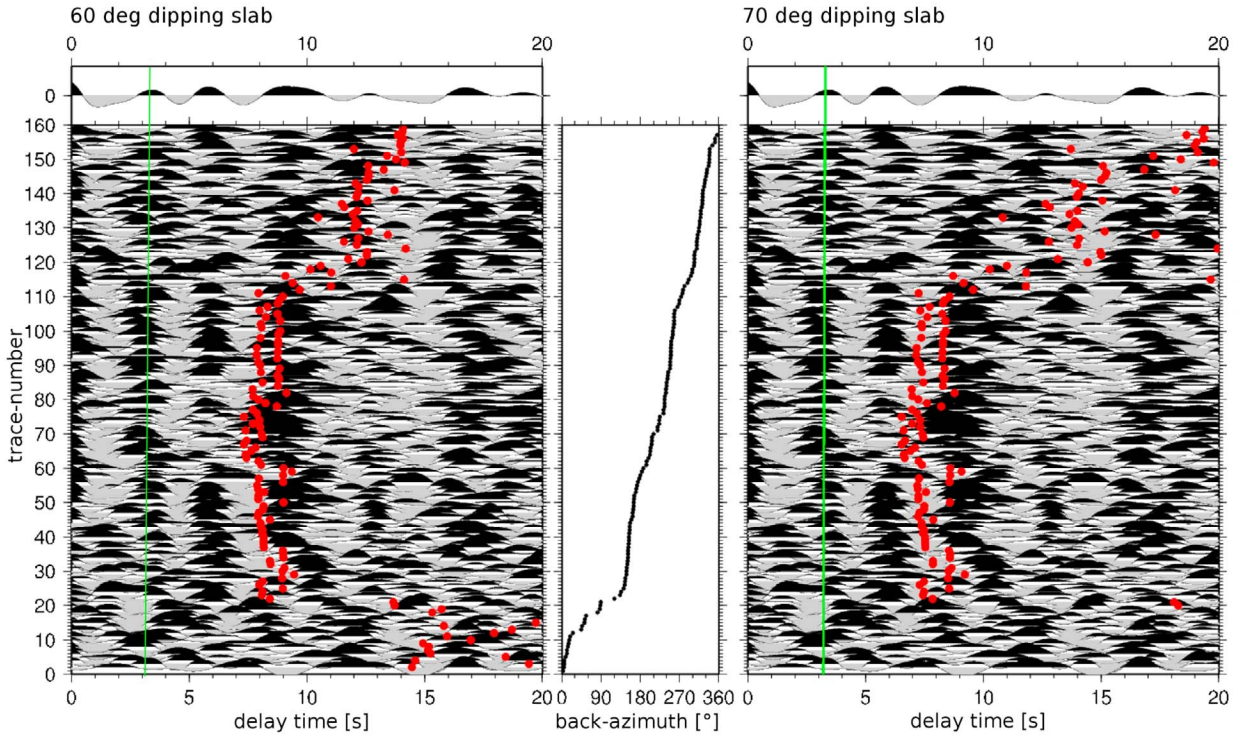

Figure A3. (a and c) Radial receiver functions (individual traces) for station crt-07, filtered with a 2 s low pass and sorted by (b) back azimuth. Representation is similar to Figure 6. The expected slab signal times were calculated for a 60° dipping slab 88 km below the station (Figure A3a) and for a 70° dipping slab at the same depth (Figure A3c). For an 80° dipping slab the signal can also be calculated to match the observations, but the downdip slab arrivals would be later than 20 s and therefore outside the range of this plot.

the case of the 80° dipping slab, our first tests showed that the contact of the slab with the Moho and crustal interface, which occurs almost directly above the dipping slab, creates a strong disruption. This is unrealistic, since we know the slab does not have such an extreme dip angle at these shallow depths. We therefore circumvented this problem by replacing the Moho and crustal interface by a velocity gradient. Thereby, the two closely spaced discontinuities are no longer present, while the average velocity is still similar to all the other models. The dipping slab is imaged clearly in both scenarios. The 60°-dipping slab produces a dipping signal of over 50°; the 80°-dipping slab creates a dipping signal of somewhat more than 60°, in agreement with the other models presented in the main text.

A4. Position of Proposed Slab Window and Receiver Function Profiles

[73] Figure A7 shows the position of the proposed slab window taken from *Abratis* [1998] for com-

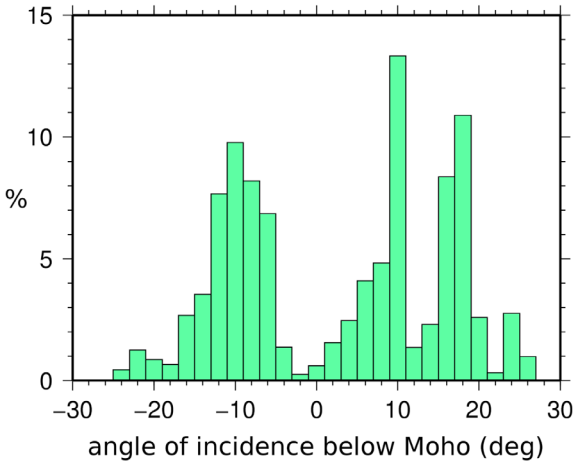

Figure A4. Distribution of angle of incidence of the analyzed receiver functions below Moho depth, after projection onto the trench-normal modeling surface (in percent).

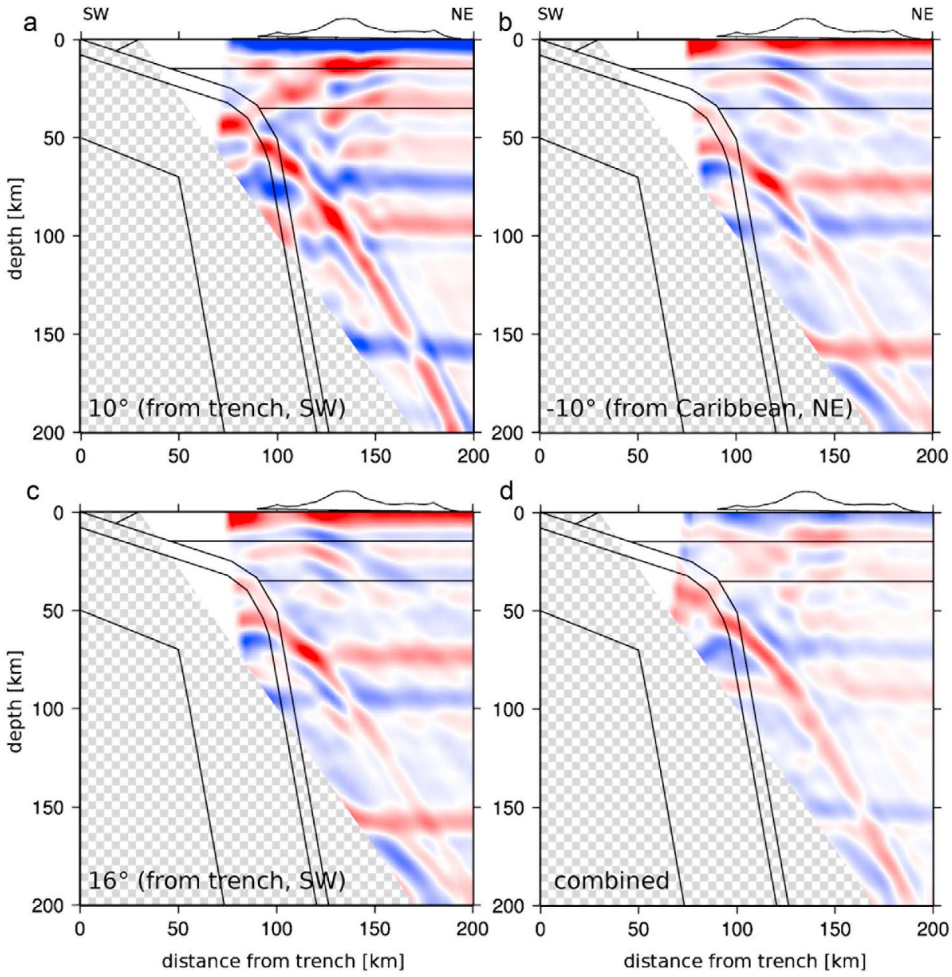

Figure A5. (a–c) Finite difference model results for slab with low-velocity crust, modeled for different angles of incidence of the incoming plane wave. (d) The combined image from a weighted sum of the different contributions. The basic model geometry is overlain as black lines. The reflection of the incoming plane wave at the model boundaries creates a group of later arriving waves coming from the side, which is shaded in the results.

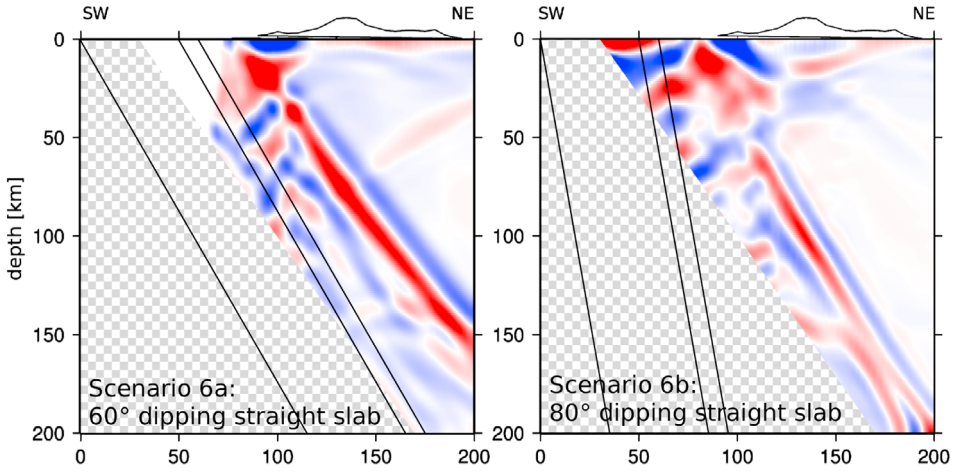

Figure A6. Finite difference model results for different scenarios to test for the effect of the "kink" in the slab between 60° and 80° dip. Details are given in the text.

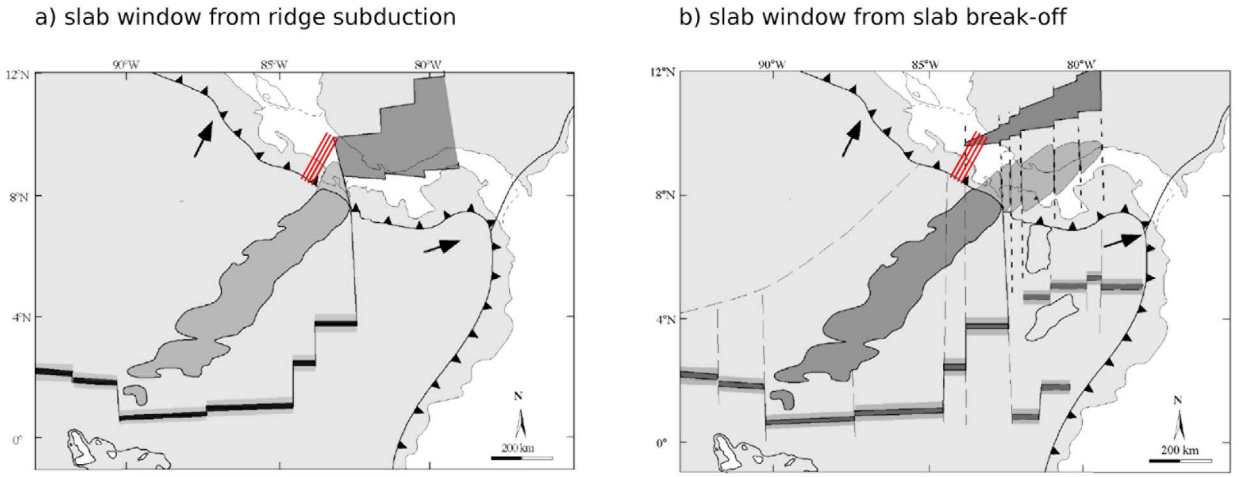

Figure A7. Position of a hypothetical slab window suggested by *Abratis* [1998] created by (a) subduction of a spreading ridge or (b) slab break-off, with position of receiver function profiles overlain in red.

parison with the receiver function study area. The hypothetical slab window in the ridge subduction scenario (Figure A7a) would occur to the south of our study area and would therefore not be visible in the receiver function profiles. For a slab window originating from slab break-off, the window would occur further to the west, under the Caribbean coast of Costa Rica. In this case, it would be placed under the northeastern edge of the receiver function profiles, at distances of 150–170 km from the trench.

Acknowledgments

[74] This work has benefited greatly from the constructive comments by three anonymous reviewers. We gratefully acknowledge many helpful discussions with R. von Huene, V. Levin, and I. Morozov on earlier versions of this manuscript. This is contribution 135 of the SFB 574 "Volatiles and Fluids in Subduction Zones" at the University of Kiel, funded by the German Research Foundation (DFG). About half of the Talamanca Transect stations were provided by the GeoForschungsZentrum Potsdam instrument pool. We thank Xiaohui Yuan for providing his codes for the receiver function analysis, which were used for the nmo correction. This research has made use of the SH (Seismic Handler), sac (Seismic Analysis Code), GMT, and Passcal software packages and of NASA's Physics/Astrophysics Data System.

References

Abers, G. A. (2005), Seismic low-velocity layer at the top of subduction slabs: Observations, predictions, and systematics, *Phys. Earth Planet. Inter.*, *149*, 7–29.

Abratis, M. (1998), Geochemical variations in magmatic rocks from southern Costa Rica as a consequence of Cocos Ridge subduction and uplift of the Cordillera de Talamanca, Ph.D. thesis, Georg-August-Universität Göttingen, Göttingen, Germany.

Abratis, M., and G. Wörner (2001), Ridge collision, slab-window formation, and the flux of Pacific asthenosphere into the Caribbean realm, *Geology*, *29*, 127–130.

Abt, D. L., K. M. Fischer, G. A. Abers, W. Strauch, J. M. Protti, and V. González (2009), Shear wave anisotropy beneath Nicaragua and Costa Rica: Implications for flow in the mantle wedge, *Geochem. Geophys. Geosyst.*, *10*, Q05S15, doi:10.1029/2009GC002375.

Adamek, S., C. Frohlich, and W. D. Pennington (1988), Seismicity of the Caribbean-Nazca plate boundary: Constraints on microplate tectonics of the Panama region, *J. Geophys. Res.*, *93*(B3), 2053–5075.

Arroyo, I. (2001), Sismicidad y Neotectónica en la región de influencia del proyecto Boruca: Hacia una mejor definición sismogénica del Sureste de Costa Rica, tesis de licenciatura, Escuela Centroam. de Geol., Univ. de Costa Rica, San José.

Barckhausen, U., C. R. Ranero, R. von Huene, S. C. Cande, and H. A. Roeser (2001), Revised tectonic boundaries in the Cocos Plate off Costa Rica: Implications for the segmentation of the convergent margin and for plate tectonic models, *J. Geophys. Res.*, *106*(B9), 19,207–19,220.

Barckhausen, U., C. R. Ranero, S. C. Cande, M. Engels, and W. Weinrebe (2008), Birth of an intraoceanic spreading center, *Geology*, *36*(10), 767–770, doi:10.1130/G2056A.1.

Bird, P. (2003), An updated digital model of plate boundaries, *Geochem. Geophys. Geosyst.*, *4*(3), 1027, doi:10.1029/2001GC000252.

Bohlen, T. (2002), Parallel 3-D viscoelastic finite-difference seismic modeling, *Comput. Geosci.*, *28*(8), 887–889.

Bostock, M. G. (1999), Seismic waves converted from velocity gradient anomalies in the Earth's upper mantle, *Geophys. J. Int.*, *137*, 747–756.

Bostock, M. G., and S. Rondenay (1999), Migration of scattered teleseismic body waves, *Geophys. J. Int.*, *137*, 732–746.

Bostock, M. G., S. Rondenay, and J. Shragge (2001), Multiparameter two-dimensional inversion of scattered teleseismic body waves: 1. Theory for oblique incidence, *J. Geophys. Res.*, *106*(12), 30,771–30,782.

Burbach, G. V., C. Frohlich, W. D. Pennington, and T. Matumoto (1984), Seismicity and tectonics of the subducted Cocos Plate, *J. Geophys. Res.*, *89*(B9), 7719–7735.

Burke, K. (1988), Tectonic evolution of the Caribbean, *Annu. Rev. Earth Planet. Sci.*, *67*, 677–691.

Camacho, E., W. Hutton, and J. F. Pacheco (2010), A new look at evidence for a Wadati-Benioff zone and active convergence at the north Panama deformed belt, *Bull. Seismol. Soc. Am.*, *100*(1), 343–348, doi:10.1785/0120090204.

Carr, M. J. (1984), Symmetrical and segmented variation of physical and geochemical characteristics of the Central American volcanic front, *J. Volcanol. Geotherm. Res.*, *20*, 231–252.

Carr, M. J., and R. E. Stoiber (1990), Volcanism (Chapter 14), in *The Geology of North America*, vol. H, *The Caribbean Region*, edited by G. Dengo and J. E. Case, chap. 14, pp. 375–391, Geol. Soc. of Am., Boulder, Colo.

Carr, M. J., L. C. Patino, and M. D. Feigenson (2007), Petrology and geochemistry of lavas, in *Central America: Geology, Resources and Hazards*, vol. 1, edited by J. Bundschuh and G. E. Alvarado, pp. 565–577, Taylor and Francis, London.

Cassidy, J. F. (1992), Numerical experiments in broadband receiver function analysis, *Bull. Seismol. Soc. Am.*, *82*(3), 1453–1474.

Collins, L. S., A. G. Coates, J. B. C. Jackson, and J. A. Obando (1995), Timing and rates of emergence of the Limón and Bocas del Toro basins: Caribbean effects of Cocos Ridge subduction?, in *Geologic and Tectonic Development of the Caribbean Plate Boundary in Southern Central America*, edited by P. Mann, *Spec. Pap. Geol. Soc. Am.*, 295, 263–289.

Conrad, C. P., S. Bilek, and C. Lithgow-Bertelloni (2004), Great earthquakes and slab pull: Interaction between seismic coupling and plate-slab coupling, *Earth Planet. Sci. Lett.*, *218*, 109–122.

Corrigan, J., P. Mann, and J. C. Ingle Jr. (1990), Forearc response to subduction of the Cocos Ridge, Panama–Costa Rica, *Geol. Soc. Am. Bull.*, *102*, 628–652.

de Boer, J. Z., M. J. Defant, R. H. Stewart, J. F. Restrepo, L. F. Clark, and A. H. Ramirez (1988), Quaternary calc-alkaline volcanism in western Panama: Regional variation and implication of the plate tectonic framework, *J. South Am. Earth Sci.*, *1*(3), 275–293.

de Boer, J. Z., M. S. Drummond, M. J. Bordelon, M. J. Defant, H. Bellon, and R. C. Maury (1995), Cenozoic magmatic phases of the Costa Rican island arc (Cordillera de Talamanca), in *Geologic and Tectonic Development of the Caribbean Plate Boundary in Southern Central America*, edited by P. Mann, *Spec. Pap. Geol. Soc. Am.*, 295, 35–56.

deMets, C., R. G. Gordon, D. F. Argus, and S. Stein (1990), Current plate motions, *Geophys. J. Int.*, *101*, 425–478.

deMets, C., R. G. Gordon, D. F. Argus, and S. Stein (1994), Effects of recent revisions to the geomagnetic reversal time scale on estimates of current plate motions, *Geophys. Res. Lett.*, *31*(20), 2191–2194.

Dengo, G. (1985), Mid America: Tectonic setting for the Pacific margin from southern Mexico to northwestern Colombia, in *The Ocean Basins and Margins*, vol. 7A, edited by A. E. Nairn and F. G. Stechli, pp. 123–180, Plenum, New York.

DeShon, H. R., S. Y. Schwartz, S. L. Bilek, L. M. Dorman, V. Gonzalez, J. M. Protti, E. R. Flueh, and T. H. Dixon (2003), Seismogenic zone structure of the southern Middle America Trench, Costa Rica, *J. Geophys. Res.*, *108*(B10), 2491, doi:10.1029/2002JB002294.

Dinc, A. N. (2008), Local earthquake tomography of Central America: Structural variations and fluid transport in the Nicaragua–Costa Rica subduction zone, Ph.D. thesis, Christian-Albrechts-Univ. zu Kiel, Kiel, Germany.

Dinc, A. N., I. Koulakov, M. Thorwart, W. Rabbel, E. Flueh, I. Arroyo, W. Taylor, and G. Alvarado (2010), Local earthquake tomography of central Costa Rica: Transition from seamount to ridge subduction, *Geophys. J. Int.*, *183*(1), 286–302, doi:10.1111/j.1365-246X.2010.04717.x.

Dzierma, Y. (2009), A receiver function study of southern Costa Rica—Indications of steep Cocos Ridge subduction, Ph.D. thesis, Christian-Albrechts-Univ. zu Kiel, Kiel, Germany.

Dzierma, Y., M. M. Thorwart, W. Rabbel, E. R. Flueh, G. E. Alvarado, and M. M. Mora (2010), Imaging crustal structure in south-central Costa Rica with receiver functions, *Geochem. Geophys. Geosyst.*, *11*, Q08S26, doi:10.1029/2009GC002936.

Efron, B., and R. Tibshirani (1986), Bootstrap methods for standard errors, confidence intervals, and other measures of statistical accuracy, *Stat. Sci.*, *1*, 54–77.

Escalante, G. (1990), The geology of southern Central America and western Colombia, in *The Geology of North America*, vol. H, *The Caribbean Region*, edited by G. Dengo and J. E. Case, chap. 8, pp. 201–228, Geol. Soc. of Am., Boulder, Colo.

Espurt, N., F. Funiciello, J. Martinod, B. Buillaume, V. Regard, C. Faccenna, and S. Brusset (2008), Flat subduction dynamics and deformation of the South American plate: Insights from analog modeling, *Tectonics*, *27*, TC3011, doi:10.1029/2007TC002175.

Feigenson, M. D., and M. J. Carr (1993), The source of Central American lavas: Inferences from geochemical inverse modeling, *Contrib. Mineral. Petrol.*, *113*, 226–235.

Fisher, D. M., T. W. Gardner, P. B. Sak, J. D. Sanchez, K. Murphy, and P. Vannucchi (2004), Active thrusting in the inner forearc of an erosive convergent margin, Pacific coast, Costa Rica, *Tectonics*, *23*, TC2007, doi:10.1029/2002TC001464.

Gardner, T. W., D. Verdonck, N. M. Pinter, R. Slingerland, K. P. Furlong, T. F. Bullard, and S. G. Wells (1992), Quaternary uplift astride the aseismic Cocos Ridge, Pacific coast, Costa Rica, *Geol. Soc. Am. Bull.*, *104*, 219–232.

Goss, A. R., and S. M. Kay (2006), Steep REE patterns and enriched Pb isotopes in southern Central American arc magmas: Evidence for forearc subduction erosion?, *Geochem. Geophys. Geosyst.*, *7*, Q05016, doi:10.1029/2005GC001163.

Gossler, J., R. Kind, S. V. Sobolev, H. Kämpf, K. Wylegalla, M. Stiller, and TOR Working Group (1999), Major crustal features between the Harz Mountains and the Baltic Shield derived from receiver functions, *Tectonophysics*, *314*, 321–333.

Gräfe, K., W. Frisch, I. M. Villa, and M. Meschede (2002), Geodynamic evolution of southern Costa Rica related to low-angle subduction of the Cocos Ridge: Constraints from thermochronology, *Tectonophysics*, *348*, 187–204.

Grevemeyer, I., C. R. Ranero, E. R. Flueh, D. Kläschen, and J. Bialas (2007), Passive and active seismological study of bending-related faulting and mantle serpentinization at the Middle America trench, *Earth Planet. Sci. Lett.*, *258*, 528–542.

Guendel, F. D. (1986), An analytical view of the southern terminus of the Middle America trench, Ph.D. thesis, 156 pp., Univ. of Calif., Santa Cruz.

Guillier, B., J.-L. Chatelain, É. Jaillard, H. Yepes, G. Poupinet, and J.-F. Fels (2001), Seismological evidence of the geometry of the orogenic system in central-northern Ecuador (South America), *Geophys. Res. Lett.*, *28*(19), 3749–3752.

Gutscher, M.-A., R. Maury, J.-P. Eissen, and E. Bourdon (2000), Geodynamics of flat subduction: Seismicity and tomographic constraints from the Andean margin, *Tectonics*, *19*(5), 814–833.

Hampel, A. (2002), The migration history of the Nazca Ridge along the Peruvian active margin: A re-evaluation, *Earth Planet. Sci. Lett.*, *203*, 665–679.

Helffrich, G. (1995), Subducted lithospheric slab velocity structure: Observations and mineralogical inferences, in *Subduction: Top to Bottom*, *Geophys. Monogr. Lett.*, vol. 96, edited by G. E. Bebout et al., pp. 215–222, AGU, Washington, D. C.

Hey, R. (1977), Tectonic evolution of the Cocos-Nazca spreading center, *Geol. Soc. Am. Bull.*, *88*, 1404–1420.

Hoernle, K., et al. (2008), Arc-parallel flow in the mantle wedge beneath Costa Rica and Nicaragua, *Nature*, *541*, 1094–1097.

Husen, S., R. Quintero, E. Kissling, and B. Hacker (2003), Subduction-zone structure and magmatic processes beneath Costa Rica constrained by local earthquake tomography and petrological modeling, *Geophys. J. Int.*, *155*, 11–32.

Ivandic, M., I. Grevemeyer, A. Berhorst, E. R. Flueh, and K. McIntosh (2008), Impact of bending related faulting on the seismic properties of the incoming oceanic plate offshore of Nicaragua, *J. Geophys. Res.*, *113*, B05410, doi:10.1029/2007JB005291.

Johnston, S. T., and D. J. Thorkelson (1997), Cocos-Nazca slab window beneath Central America, *Earth Planet. Sci. Lett.*, *146*, 465–474.

Jones, C. H., and R. A. Phinney (1998), Seismic structure of the lithosphere from teleseismic converted arrivals observed at small arrays in the southern Sierra Nevada and vicinity, *J. Geophys. Res.*, *103*, 10,065–10,090.

Kellogg, J. N., and V. Vega (1995), Tectonic development of Panama, Costa Rica, and the Colombian Andes: Constraints from Global Positioning System geodetic studies and gravity, in *Geologic and Tectonic Development of the Caribbean Plate Boundary in Southern Central America*, edited by P. Mann, *Spec. Pap. Geol. Soc. Am.*, 295, 75–90.

Kind, R., G. L. Kosarev, and N. V. Petersen (1995), Receiver functions at the stations of the German Regional Seismic Network (GRSN), *Geophys. J. Int.*, *62*, 191–202.

Kirby, S., E. R. Engdahl, and R. Denlinger (1996), Intermediate-depth intraslab earthquakes and arc volcanism as physical expressions of crustal and uppermost mantle metamorphism in subducting slabs, in *Subduction: Top to Bottom*, *Geophys. Monogr. Ser.*, vol. 96, edited by G. E. Bebout et al., pp. 195–214, AGU, Washington, D. C.

Kokfelt, T. F., C. Lundstrom, K. Hoernle, F. Hauff, and R. Werner (2005), Plume-ridge interaction studied at the Galápagos spreading center: Evidence from ^{226}Ra–^{230}Th–^{235}U isotopic disequilibria, *Earth Planet. Sci. Lett.*, *234*, 165–187.

Kolarsky, R. A., P. Mann, and W. Montero (1995), Island arc response to shallow subduction of the Cocos Ridge, Costa Rica, in *Geologic and Tectonic Development of the Caribbean Plate Boundary in Southern Central America*, edited by P. Mann, *Spec. Pap. Geol. Soc. Am.*, 295, 235–262.

Kosarev, G., R. Kind, S. V. Sobolev, X. Yuan, W. Hanka, and S. Oreshin (1999), Seismic evidence for a detached Indian lithospheric mantle beneath Tibet, *Science*, *283*, 1306–1309.

LaFemina, P., T. H. Dixon, R. Govers, E. Norabuena, H. Turner, A. Saballos, G. Mattioli, M. Protti, and W. Strauch (2009), Fore-arc motion and Cocos Ridge collision in Central America, *Geochem. Geophys. Geosyst.*, *10*, Q05S14, doi:10.1029/2008GC002181.

Leeman, W. P., M. J. Carr, and J. D. Morris (1994), Boron geochemistry of the Central American Volcanic Arc: Constraints on the genesis of subduction-related magmas, *Geochim. Cosmochim. Acta*, *58*, 149–168.

Lewis, J. C., A. C. Boozer, A. López, and W. Montero (2008), Collision versus sliver transport in the hanging wall at the Middle America subduction zone: Constraints from background seismicity in central Costa Rica, *Geochem. Geophys. Geosyst.*, *9*, Q07S06, doi:10.1029/2007GC001711.

Lonsdale, P., and K. D. Klitgord (1978), Structure and tectonic history of the eastern Panama Basin, *Geol. Soc. Am. Bull.*, *89*, 981–999.

MacKenzie, L. S., G. A. Abers, S. Rondenay, and K. M. Fischer (2010), Imaging a steeply dipping subducting slab in southern Central America, *Earth Planet. Sci. Lett.*, *296*, 459–468, doi:10.1016/j.epsl.2010.05.033.

MacMillan, I., P. B. Gans, and G. Alvarado (2004), Middle Miocene to present plate tectonic history of the southern Central American Volcanic Arc, *Tectonophysics*, *392*(1–4), 325–348.

Mann, P., R. D. Rogers, and L. Gahagan (2007), Overview of plate tectonic history and its unresolved tectonic problems, in *Central America: Geology, Resources and Hazards*, vol. 1, edited by G. Alvarado and J. Buntschuh, chap. 8, pp. 201–237, Taylor and Francis, London.

Marshall, J. S., D. M. Fisher, and T. W. Gardner (2000), Central Costa Rica deformed belt: Kinematics of diffuse faulting across the western Panama block, *Tectonics*, *19*(3), 468–492.

McGeary, S., A. Nur, and Z. Ben-Avraham (1985), Spatial gaps in arc volcanism: The effect of collision or subduction of oceanic plateaus, *Tectonophysics*, *119*, 195–221.

Meschede, M., and U. Barckhausen (2000), Plate tectonic evolution of the Cocos-Nazca Spreading Center [online], *Proc. Ocean Drill. Program Sci. Results*, *170*, 10 pp. (Available at http://www-odp.tamu.edu/publications/170_SR/VOLUME/CHAPTERS/SR170_07.PDF.)

Meschede, M., U. Barckhausen, and H.-U. Worm (1998), Extinct spreading on the Cocos Ridge, *Terra Nova*, *10*(4), 211–216.

Montero, W. (2001), Neotectónica de la región central de Costa Rica: Frontera oeste de la microplaca de Panamá, *Rev. Geol. Am. Cent.*, *24*, 29–56.

Morozov, I. B. (2004), Crustal scattering and some artifacts in receiver function images, *Bull. Seismol. Soc. Am.*, *94*(4), 1492–1499.

Morozov, I. B., and H. Zheng (2006), Effects of trench-zone scattering on receiver functions over a subduction zone: A 3-D finite-difference modeling study, *Tectonophysics*, *420*, 317–332.

Nur, A., and Z. Ben-Avraham (1983), Volcanic gaps due to oblique consumption of aseismic ridges, *Tectonophysics*, *99*, 355–362.

Owens, T. J., G. Zandt, and S. R. Taylor (1984), Seismic evidence for an ancient rift beneath the Cumberland Plateau, Tennessee: A detailed analysis of broadband teleseismic P waveforms, *J. Geophys. Res.*, *89*(B9), 7783–7795.

Pardo, M., D. Comte, and T. Monfret (2002), Seismotectonic and stress distribution in the central Chile subduction zone, *J. South Am. Earth Sci.*, *15*, 11–22.

Peacock, S. M., P. E. van Keken, S. D. Holloway, B. R. Hacker, G. A. Abers, and R. L. Fergason (2004), Thermal structure of the Costa Rica–Nicaragua subduction zone, *Phys. Earth Planet. Inter.*, *149*(1–2), 187–200.

Phipps Morgan, J., C. R. Ranero, and P. Vannucchi (2008), Intra-arc extension in Central America: Links between plate motions, tectonics, volcanism, and geochemistry, *Earth Planet. Sci. Lett.*, *272*, 365–371.

Pilger, R. H. (1981), Plate reconstructions, aseismic ridges, and low-angle subduction beneath the Andes, *Geol. Soc. Am. Bull.*, *92*, 448–456.

Protti, M., F. Guendel, and K. McNally (1994), The geometry of the Wadati-Benioff zone under southern Central America and its tectonic significance: Results from a high-resolution local seismographic network, *Phys. Earth Planet. Inter.*, *84*, 271–287.

Protti, M., F. Guendel, and K. McNally (1995), Correlation between the age of the subducting Cocos plate and the geometry of the Wadati-Benioff zone under Nicaragua and Costa Rica, in *Geologic and Tectonic Development of the Caribbean Plate Boundary in Southern Central America*, edited by P. Mann, *Spec. Pap. Geol. Soc. Am.*, 295, 309–326.

Quintero, R., and E. Kissling (2001), An improved P-wave velocity reference model for Costa Rica, *Geofis. Int.*, *40*(1), 3–19.

Ramesh, D. S., H. Kawakatsu, S. Watada, and X. Yuan (2005), Receiver function images of the central Chugoku region in the Japanese islands using Hi-net data, *Earth Planets Space*, *57*, 271–280.

Ramos, V. A., E. O. Cristallini, and D. J. Pérez (2002), The Pampean flat-slab of the central Andes, *J. South Am. Earth Sci.*, *15*, 59–78.

Rondenay, S., M. G. Bostock, and J. Shragge (2001), Multiparameter two-dimensional inversion of scattered teleseismic body waves: 3. Application to the Cascadia 1993 data set, *J. Geophys. Res.*, *106*(12), 30,795–30,807.

Rosenbaum, G., D. Giles, M. Saxon, P. G. Betts, R. F. Weinberg, and C. Duboz (2005), Subduction of the Nazca Ridge and the Inca Plateau: Insights into the formation of ore deposits in Peru, *Earth Planet. Sci. Lett.*, *239*, 18–32.

Rüpke, L. H., J. Phipps Morgan, M. Hort, and J. A. D. Connolly (2002), Are the regional variations in Central American arc lavas due to differing basaltic versus peridotitic slab sources of fluids?, *Geology*, *30*(11), 1035–1038.

Sallarès, V., P. Charvis, E. R. Flueh, and J. Bialas (2003), Seismic structure of Cocos and Malpelo Volcanic Ridges and implications for hot spot-ridge interaction, *J. Geophys. Res.*, *108*(B12), 2564, doi:10.1029/2003JB002431.

Savage, M. K. (1998), Lower crustal anisotropy or dipping boundaries? Effects on receiver functions and a case study in New Zealand, *J. Geophys. Res.*, *103*(B7), 15,069–15,087.

Schlindwein, V. (2001), Azimuthal variation of the P phase in Icelandic receiver functions, *Geophys. J. Int.*, *144*, 221–230.

Shragge, J., M. G. Bostock, and S. Rondenay (2001), Multiparameter two-dimensional inversion of scattered teleseismic body waves: 2. Numerical examples, *J. Geophys. Res.*, *106*(12), 30,783–30,793.

Silver, E. A., D. L. Reed, J. E. Tagudin, and J. Heil (1990), Implications of the north and south Panama thrust belts for the origin of the Panama orocline, *Tectonics*, *9*, 261–281.

Sitchler, J. C., D. M. Fisher, T. W. Gardner, and M. Protti (2007), Constraints on inner forearc deformation from balanced cross sections, Fila Costeña thrust belt, Costa Rica, *Tectonics*, *26*, TC6012, doi:10.1029/2006TC001949.

Stavenhagen, A. U. (1998), Refraktionsseismische Untersuchungen on- und offshore Costa Rica, Ph.D. thesis, Christian-Albrechts-Univ. zu Kiel, Kiel, Germany.

Stavenhagen, A. U., E. R. Flueh, C. Ranero, K. D. McIntosh, T. Shipley, G. Leandro, A. Schulze, and J. J. Dañobeitia (1998), Seismic wide-angle investigations in Costa Rica—A crustal velocity model from the Pacific to the Caribbean coast, *Zeitbl. Geol. Palaeontol.*, *Part 1*, 3–6, 393–408.

Tassara, A., H.-J. Götze, S. Schmidt, and R. Hackney (2006), Three-dimensional density model of the Nazca plate and the Andean continental margin, *J. Geophys. Res.*, *111*, B09404, doi:10.1029/2005JB003976.

Vannucchi, P., D. M. Fisher, S. Bier, and T. W. Gardner (2006), From seamount accretion to tectonic erosion: Formation of Osa Mélange and the effects of Cocos Ridge subduction in southern Costa Rica, *Tectonics*, *25*, TC2004, doi:10.1029/2005TC001855.

Vinnik, L. P. (1977), Detection of waves converted from P to SV in the mantle, *Phys. Earth Planet. Inter.*, *15*, 294–303.

Vogt, P. R. (1973), Subduction and Aseismic Ridges, *Nature*, *241*, 189–191.

von Huene, R., et al. (1995), Morphotectonics of the Pacific convergent margin of Costa Rica, in *Geologic and Tectonic Development of the Caribbean Plate Boundary in Southern Central America*, edited by P. Mann, *Spec. Pap. Geol. Soc.Am.*, 295, 291–308.

von Huene, R., C. R. Ranero, and W. Weinrebe (2000), Quaternary convergent margin tectonics of Costa Rica, segmentation of the Cocos Plate, and Central American volcanism, *Tectonics*, *19*(2), 314–334.

Walther, C. H. E. (2003), The crustal structure of the Cocos ridge off Costa Rica, *J. Geophys. Res.*, *108*(B3), 2136, doi:10.1029/2001JB000888.

Werner, R., K. Hoernle, P. van den Bogaard, C. Ranero, R. von Huene, and D. Korish (1999), Drowned 14-m.y.-old Galápagos archipelago off the coast of Costa Rica: Implications for tectonic and evolutionary models, *Geology*, *27*(6), 499–502.

Yamauchi, M., K. Hirahara, and T. Shibutani (2003), High resolution receiver function imaging of the seismic velocity discontinuities in the crust and uppermost mantle beneath southwest Japan, *Earth Planets Space*, *55*, 59–64.

Yañez, G. A., C. R. Ranero, R. von Huene, and J. Díaz (2001), Magnetic anomaly interpretation across the southern central Andes (32°–34°S): The role of the Juan Fernández Ridge in the late Tertiary evolution of the margin, *J. Geophys. Res.*, *106*(B4), 6325–6345.

Yuan, X., et al. (2000), Subduction and collision processes in the central Andes constrained by converted seismic phases, *Nature*, *408*, 958–961.